

# 1 **Characterization of atmospheric trace gases and particulate matters** 2 **in Hangzhou, China**

3 Gen Zhang<sup>1</sup>, Honghui Xu<sup>2</sup>, Bing Qi<sup>3</sup>, Rongguang Du<sup>3</sup>, Ke Gui<sup>1</sup>, Hongli Wang<sup>4</sup>, Wanting Jiang<sup>5</sup>, Linlin  
4 Liang<sup>1</sup>, Wanyun Xu<sup>1</sup>

5 <sup>1</sup>State Key Laboratory of Severe Weather & Key Laboratory of Atmospheric Chemistry of CMA, Chinese Academy of  
6 Meteorological Sciences, Beijing 100081, China

7 <sup>2</sup>Zhejiang Institute of Meteorological Science, Hangzhou 310008, China

8 <sup>3</sup>Hangzhou Meteorological Bureau, Hangzhou 310051, China

9 <sup>4</sup>State Environmental Protection Key Laboratory of Formation and Prevention of Urban Air Pollution Complex, Shanghai  
10 Academy of Environmental Sciences, Shanghai 200233, China

11 <sup>5</sup>Plateau Atmospheric and Environment Laboratory of Sichuan Province, College of Atmospheric Science, Chengdu  
12 University of Information Technology, Chengdu 610225, China

13 *Correspondence to:* Gen Zhang (zhanggen@cma.gov.cn) and Honghui Xu (forsnow@126.com)

14 **Abstract.** The Yangtze River Delta (YRD) is one of the most densely populated regions in China with severe air quality  
15 issues, which has not been fully understood. Thus, in this study, based on one-year (2013) continuous measurement at a  
16 National Reference Climatological Station (NRCS, 30.22°N, 120.17°E, 41.7 m a. s. l) in the center of Hangzhou in the YRD,  
17 we investigated the seasonal characteristics, interspecies relationships, and the local emissions and the regional potential  
18 source contributions of trace gases (including O<sub>3</sub>, NO<sub>x</sub>, NO<sub>y</sub>, SO<sub>2</sub> and CO) and particulate matters (PM<sub>2.5</sub> and PM<sub>10</sub>). Results  
19 revealed severe two-tier air pollution (photochemical and haze pollution) occurred in this region, with frequent exceedances  
20 in O<sub>3</sub> (38 days) and PM<sub>2.5</sub> (62 days). O<sub>3</sub> and PM<sub>2.5</sub> both exhibited distinct seasonal variations with reversed patterns: O<sub>3</sub>  
21 reaching a maximum in warm seasons (May and July) but PM<sub>2.5</sub> in cold seasons (November to January). The overall results  
22 from interspecies correlation indicated a strong local photochemistry favoring the O<sub>3</sub> production under a volatile organic  
23 compound (VOC)-limited regime, whereas it moved towards an optimum O<sub>3</sub> production zone during warm seasons,  
24 accompanying with a formation of secondary fine particulates under high O<sub>3</sub>. The emission maps of PM<sub>2.5</sub>, CO, NO<sub>x</sub>, and  
25 SO<sub>2</sub> demonstrated that local emissions were both significant for these species on seasonal scale. The contributions from the  
26 regional transports among inland cities (Zhejiang, Jiangsu, Anhui, and Jiangxi Province) on seasonal scale were further  
27 confirmed to be crucial to air pollution at NRCS site by using the backward trajectories simulations. Air masses transported  
28 from the offshore area of Yellow Sea, East Sea, and South Sea were also found to be highly relevant to the elevated O<sub>3</sub> at  
29 NRCS site through the analysis of potential source contribution function (PSCF). Case studies of photochemical pollution  
30 (O<sub>3</sub>) and haze (PM<sub>2.5</sub>) episodes both suggested the combined importance of local atmospheric photochemistry and synoptic  
31 conditions during the accumulation (related with anticyclones) and dilution process (related with cyclones). Apart from

32 supplementing a general picture of the air pollution state in urban Hangzhou in the YRD region, this study specifically  
33 elucidates the role of local emission and regional transport, and interprets the physical and photochemical processes during  
34 haze and photochemical pollution episodes. Moreover, this work suggests that cross-regional control measures are crucial to  
35 improve air quality in the YRD region, and further emphasizes the importance of local thermally induced circulation on air  
36 quality.

## 37 **1 Introduction**

38 Ambient air quality is mainly affected by particulate matters ( $PM_{2.5}$  and  $PM_{10}$ ) and gaseous pollutants such as ozone ( $O_3$ ),  
39 nitrogen oxides ( $NO_x$ ), carbon monoxide (CO), and sulfur dioxide ( $SO_2$ ). Particulate matters are both from natural sources  
40 (e.g., windborne dust, volcanoes) or anthropogenic activities such as fossil and biomass fuel combustion (Chow and Watson,  
41 2002). In addition to the net downward transport of  $O_3$  by eddy diffusion from the stratosphere aloft, tropospheric  $O_3$  is a  
42 well-known secondary gaseous pollutant and formed through the photochemical oxidation of volatile organic compounds  
43 (VOCs) and  $NO_x$  under the irradiation of sunlight (Logan, 1985; Roelofs et al., 1997). These chemicals both have received  
44 extensive attention either due to their harmful impact on human health (Pope et al., 1999; Shao et al., 2006; Streets et al.,  
45 2007; Liu et al., 2013) and vegetation (Feng et al., 2014) or significant effects on climate change (Seinfeld et al., 2004; IPCC,  
46 2007; Mercado et al., 2009). Moreover, some critical interactions have been verified existing between the gaseous pollutants  
47 and/or particulate matters (Zhang et al., 2004; Cheng et al., 2016). For instance, in the presence of high  $NH_3$  and low air  
48 temperature, ammonium nitrate ( $NH_4NO_3$ ) is formed in regions with  $HNO_3$  and  $NH_3$ , which is an important constituent of  
49  $PM_{2.5}$  under the high  $NO_x$  condition (Seinfeld and Pandis, 2006). To some extent, such interactions further improve or  
50 deteriorate the air quality. The oxidation of  $SO_2$  leads to acid deposition but also contributes to the formation of sulphate  
51 aerosols (Meagher et al., 1978; Saxena and Seigneur, 1987), which in turn will influence the solar radiation and  
52 photochemistry (Dickerson et al., 1997) and further weaken the formation of secondary pollutants. Therefore, clear  
53 understanding in their characteristics, sources, transport, and formation mechanisms including interactions is crucial for  
54 gaining the comprehensive information on the complex air pollution.

55 The Yangtze River Delta (YRD) region is located in the eastern of China, including the mega-city Shanghai and the well-  
56 industrialized areas of southern Jiangsu Province and northern Zhejiang Province, with over ten large cities such as  
57 Hangzhou, Suzhou, Wuxi and Changzhou lying along the mid-YRD (Fig. 1). Being one of the most rapid growths of  
58 transportation, industries, and urbanization regions in China, it has been become hot spot with air pollution over the past  
59 three decades, together with the Pearl River Delta (PRD) and Beijing-Tianjin-Hebei (BTH) region. To date, numerous  
60 combined studies of  $O_3$  and  $PM_{2.5}$  were implemented in representative urban cities in YRD region such as Shanghai (Geng et  
61 al., 2007; Ding et al., 2013; Li et al., 2016a; Miao et al., 2017a) and Nanjing (Wang et al., 2002; Wang et al., 2003; Kang et  
62 al., 2013; Chen et al., 2016). On the contrary, in Hangzhou (29.25°-30.5°N, 118.34°-120.75°E), a capital city of Zhejiang  
63 Province in YRD region, which is lying along the mid-YRD, only a few sole studies of  $PM_{2.5}$  or  $O_3$  were sporadically  
64 conducted.  $PM_{2.5}$  measurements in urban Hangzhou have been performed only in the past five years, mostly covering short-

65 term period in winter (Jansen et al., 2014; Yu et al., 2014; Liu et al., 2015; Wu et al., 2016). Furthermore, there was still  
66 certain discrepancy about the origin of PM<sub>2.5</sub>. Wu et al. (2016a) concluded that the local vehicle emission was a major  
67 contribution to PM<sub>2.5</sub>, while results from Yu et al. (2014) suggested cross-border transports rather than local emissions  
68 control high PM<sub>2.5</sub> concentration and formation. Similarly, the photochemical pollution in urban Hangzhou was also not well  
69 understood. To our knowledge, the pioneer measurement of O<sub>3</sub> in or around Hangzhou started in the 1990s at Lin'an site, a  
70 regional station located in the eastern Zhejiang Province (50 km away from Hangzhou) (Luo et al., 2000). Subsequent  
71 studies at this site depicted the first picture of the seasonal variations of O<sub>3</sub> and its precursors (Wang et al., 2001; Wang et al.,  
72 2004). In urban Hangzhou, only short-term measurements of O<sub>3</sub> were recently made during the summertime of 2013 (Li et  
73 al., 2017). Hence, there are large knowledge gap on seasonal characteristics of these pollutants and discrepancy on their  
74 origin, which are both crucial for fully understanding the complex combined pollution of PM<sub>2.5</sub> and O<sub>3</sub> in urban Hangzhou.

75 To supplement the seasonal picture of air pollution in YRD, we conducted continuous measurements of trace gases (O<sub>3</sub>,  
76 NO<sub>x</sub>, NO<sub>y</sub>, CO, and SO<sub>2</sub>) and particulate matters (PM<sub>2.5</sub> and PM<sub>10</sub>) during January-December 2013 at a regional site NRCS  
77 (National Reference Climatological Station) in Hangzhou, which is also an integrated measurement site for the research of  
78 climate change and atmospheric environment. This study presents the first results of one-year measurements of trace gases  
79 and particulate matters in urban Hangzhou, investigates the characteristics and cause of these chemicals by discussing their  
80 seasonal characteristics, interspecies correlations, the concentration dependence on local emission and regional transport, and  
81 the specific photochemical pollution and haze case, respectively.

## 82 **2 Experiment and meteorological conditions**

### 83 **2.1 Site description**

84 Hangzhou is situated in the eastern coast of China and is one of the most developed cities in the Yangtze River Delta region.  
85 It has 8.9 million population and 2.7 million vehicles according to the 2014 Statistical Bulletin of Hangzhou. It belongs to  
86 the subtropical monsoon climate, with an average temperature of 17.0°C, relative humidity of 75% and rainfall of 1438 mm  
87 over the past 30 years (1981-2010). In this study, all in-situ measurements of gaseous constituents, particulates and  
88 meteorological factors were conducted at a site named NRCS (30.22°N, 120.17°E, 41.7 m a.s.l) in the center of Hangzhou  
89 (Fig. 1). As a typical urban site, NRCS station is situated in the commercial and residential areas in the southern Hangzhou  
90 and thus it's characterized as a polluted receptor site as it receives local urban plumes and regional air masses from the YRD  
91 region when northwesterly wind prevails. Moreover, as the right top map shown in Fig. 1, the site is adjacent to Prince Bay  
92 Park (area, 0.8 km<sup>2</sup>) and situated in the northeastern part of West Lake famous scenic spot (area, 49 km<sup>2</sup>). Therefore it can  
93 also capture the signature of vegetation emission in urban Hangzhou under southwesterly winds. Moreover, there are no  
94 local industrial pollution sources around the site. In brief, this site can be representative of urban Hangzhou.

95

## 96 **2.2 Measurements description**

97 Measurements of trace gases, aerosols, and meteorological parameters were conducted at NRCS station during January-  
98 December 2013. Trace gases including O<sub>3</sub> and SO<sub>2</sub> were detected by a set of commercial trace gas analyzers (Thermo  
99 Environmental Instruments Inc., USA i-series 49i, 43i), respectively, with a resolution of 1 min. NO and NO<sub>x</sub> were detected  
100 by a chemiluminescence analyzer coupled with an internal MoO catalytic converter (TEI, 42i). Note that the differentiated  
101 value of NO<sub>2</sub> from NO<sub>x</sub> and NO represents the upper limit concentration of atmospheric NO<sub>2</sub> due to the interference of other  
102 nitrogen-containing components (e.g., PAN, HNO<sub>3</sub>, and HONO) in the conversion. Similar with NO<sub>x</sub>, NO<sub>y</sub> was also detected  
103 by a chemiluminescence analyzer (TEI 42i-Y) but equipped with an external MoO catalytic converter. CO was monitored  
104 with a gas filter correlation, infrared absorption analyser (TEI, 48i), with automatic zeroing every 6 hours. All the  
105 instruments are housed on the top floor of a laboratory building, which sits on the top of a hill about 40 m above the ground  
106 level. Ambient air was drawn from the 1.5 m above the rooftop to the laboratory building through a manifold connected to  
107 O<sub>3</sub>, SO<sub>2</sub>, NO and CO analyzers with PFA Teflon tubes (inside diameter: 2 cm). A separate sample line with a MoO converter  
108 was used for NO<sub>y</sub> analyzer. All trace gas analyzers were weekly span and daily zero checked except CO, and multi-point  
109 calibration was made once a month.

110 Ambient PM<sub>2.5</sub> samples were collected using co-located Thermo Scientific (formerly R&P) Model 1405D samplers. The  
111 sensor unit contains the two mass measurement hardware systems that monitor particulates that continuously accumulate on  
112 the system's exchangeable TEOM filters. PM-Coarse and PM<sub>2.5</sub> particulate, split by a virtual impactor, each accumulate on  
113 the system's exchangeable TEOM filters. By maintaining a flow rate of 1.67 L·min<sup>-1</sup> through the coarse sample flow channel  
114 and 3 L·min<sup>-1</sup> through the PM<sub>2.5</sub> sample channel, and measuring the total mass accumulated on each of the TEOM filters, the  
115 device can calculate the mass concentration of both the PM<sub>2.5</sub> and PM Coarse sample streams in near real-time. TEOM filters  
116 must be replaced before the filter loading percentage reaches 80% to ensure the quality of the data generated by the  
117 instrument. For PM, the precisions of this instrument were 2.0 µg cm<sup>-3</sup> for 1 h average and 1.0 µg cm<sup>-3</sup> for 24 h average.

## 118 **2.3 Meteorological characteristic**

119 Table 1 shows the monthly averaged meteorological parameters at NRCS station, suggesting distinct characteristics of air  
120 temperature in winter and summer in this region, with monthly averages from ca. 5 °C in January to ca. 32 °C in July. High  
121 relative humidity (RH) and a large amount of rainfall appeared in June (346 mm in total), and oppositely less precipitation  
122 and low RH in autumn and winter. Note that the seemed high RH and large rainfall occurred in October was due to an  
123 extremely synoptic event on 7 October, 2013 with the daily total rainfall of 91 mm. In addition, the wind rose implied that  
124 the prevailing wind was from northwest in autumn, north in winter, and from southwest in spring and summer (See Fig. S1  
125 in the Supplement).

126

## 127 2.4 Methodology

### 128 2.4.1 Air mass back trajectory cluster

129 In this study, 72-h back trajectories starting at the arrival level of 100 m from NRCS sites were calculated by using the  
130 National Oceanic and Atmospheric Administration (NOAA) HYSPLIT-4 model with a  $1^\circ \times 1^\circ$  grid and the final  
131 meteorological database. The six hourly final archive data were obtained from the National Center for Environmental  
132 Prediction's Global Data Assimilation System (GDAS) wind field reanalysis. GDAS uses a spectral medium-range forecast  
133 model. More details could be found at <http://www.arl.noaa.gov/ready/open/hysplit4.html>. The model was run four times per  
134 day at starting times of 00:00, 6:00, 12:00, and 18:00 UTC (08:00, 14:00, 20:00, and 02:00 LT, respectively). The method  
135 used in trajectory clustering was based on the GIS-based software TrajStat (Wang et al. 2004).

### 136 2.4.2 Potential source contribution function

137 The potential source contribution function (PSCF) is widely used to identify regional sources based on the HYSPLIT model.  
138 The zone of concern is divided into  $i \times j$  small equal grid cells. The PSCF value in the  $ij$ -th cell is defined as  $m_{ij}/n_{ij}$ , where  $n_{ij}$   
139 is denoted as the numbers of endpoints that fall in the  $ij$ -th cell and  $m_{ij}$  represents the numbers of "polluted" trajectory  
140 endpoints in the  $ij$ -th cell. In this analysis, average concentrations were considered as the "polluted" threshold (Hsu et al.,  
141 2003; Zhang et al., 2013). To minimize the effect of small values of  $n_{ij}$ , following the method of Polissar et al. (1999), the  
142 seasonal PSCF values were multiplied by arbitrary seasonal weight functions  $W_{ij}$ , expressed by WPSCF, to better reflect the  
143 uncertainty in the values for these cells. Geographic areas covered by more than 95% of the back trajectories are selected as  
144 the study domain. In this study, our study domain was in the range of  $15$ - $55^\circ\text{N}$  and  $105$ - $135^\circ\text{E}$ . The resolution was  $0.5^\circ \times 0.5^\circ$ .

$$145 \quad W_{ij(\text{spring})} = \begin{cases} 1.00 & 36 < n_{ij} \\ 0.70 & 12 < n_{ij} \leq 36 \\ 0.42 & 6 < n_{ij} \leq 12 \\ 0.17 & n_{ij} \leq 6 \end{cases} \quad W_{ij(\text{summer})} = \begin{cases} 1.00 & 42 < n_{ij} \\ 0.70 & 14 < n_{ij} \leq 42 \\ 0.42 & 7 < n_{ij} \leq 14 \\ 0.17 & n_{ij} \leq 7 \end{cases}$$
$$146 \quad W_{ij(\text{autumn})} = \begin{cases} 1.00 & 36 < n_{ij} \\ 0.70 & 12 < n_{ij} \leq 36 \\ 0.42 & 6 < n_{ij} \leq 12 \\ 0.17 & n_{ij} \leq 6 \end{cases} \quad W_{ij(\text{winter})} = \begin{cases} 1.00 & 54 < n_{ij} \\ 0.70 & 18 < n_{ij} \leq 54 \\ 0.42 & 9 < n_{ij} \leq 18 \\ 0.17 & n_{ij} \leq 9 \end{cases}$$

147 Moreover, to better elucidate the local and regional contribution to pollutants concentrations, we further compared the  
148 WPSCF results with their corresponding emission inventories of  $\text{PM}_{2.5}$ ,  $\text{CO}$ ,  $\text{NO}_x$ , and  $\text{SO}_2$  in 2013 provided by Peking  
149 University (<http://inventory.pku.edu.cn/>), which were estimated by using a bottom-up approach with  $0.1^\circ \times 0.1^\circ$  spatial  
150 resolution (Wang et al., 2013; Huang et al., 2014; Zhong et al., 2014), respectively.

### 151 2.4.3 Geopotential height (GH)

152 The geopotential height (GH) fields derived from the National Center for Environmental Prediction (NCEP) global Final  
153 (FNL) reanalysis (<http://rda.ucar.edu/datasets/ds083.2/>) are typically used to classify the synoptic types (Miao et al., 2017b).  
154 In this study, daily GH fields at the 925 hPa level from the NCEP-FNL reanalysis covering the region (100-135 °E, 20-50 °N)  
155 were classified to the prevailing synoptic types during photochemical pollution and haze episodes as discussed in Section 3.5.  
156 The NCEP-FNL reanalysis was produced from the Global Data Assimilation System, which continuously assimilates  
157 observations from the Global Telecommunication System and other sources. The NCEP-FNL reanalysis fields were on  $1^{\circ} \times 1^{\circ}$   
158 grids with a 6 h resolution.

## 159 3 Results and discussion

### 160 3.1 Concentration levels

161 To evaluate the overall concentration level of gaseous and particulate pollution at NRCS, we selected a Grade II standard of  
162 the Chinese Ambient Air Quality Standards (CAAQS, GB 3095-2012), which was released in 2012 by the China State  
163 Council and implemented thorough the whole nation in 2016 (MEP, 2012). Inferred from the Grade II CAAQS for  $PM_{2.5}$  (75  
164  $\mu\text{g m}^{-3}$  for 24 h average) and  $PM_{10}$  (150  $\mu\text{g m}^{-3}$  for 24 h average), 62 days and 26 days of  $PM_{2.5}$  and  $PM_{10}$  exceedances with  
165 daily average of 102.2  $\mu\text{g m}^{-3}$  and 195.3  $\mu\text{g m}^{-3}$  were classified thorough the period, respectively, mostly occurred in winter.  
166 For  $O_3$ , about 38 days exceedances (75 ppbv for daily maximum 8 h average for the Grade II CAAQS) in whole were found  
167 during the whole period, mostly covering from May to September. It suggested Hangzhou was suffering from heavy haze  
168 and photochemical pollution in cold and warm seasons. Concerning  $SO_2$ , the annual mean was 10.9 ppbv in this study,  
169 nearly half of the yearly mean of  $SO_2$  Grade II CAAQS (21 ppbv). It was reasonably attributed to the powerful measure of  
170 Chinese government to control the emission of  $SO_2$  starting at 1990 (He et al., 2002; Qi et al., 2012). Table 2 summarized a  
171 statistical analysis on these species and listed the comparison with the previous results in other typical regions in China. In  
172 general, with respect to all these chemicals, our results were generally comparable with those observed by other  
173 contemporaneous measurements in Hangzhou and the other cities in YRD. As expected, regional differences among YRD,  
174 PRD, and BTH could be also found as illustrated in Table 2. For instance, observed  $PM_{2.5}$ ,  $PM_{10}$ , and CO concentrations  
175 were higher in BTH than those in YRD and PRD through the comparison among provincial capital cities in China during  
176 2011-2014 (Chai et al., 2014; Wang et al., 2014), which has been extrapolated to be more emissions from coal-based  
177 industries and coal and biomass burning based domestic home heating in BTH in winter (Zhang et al., 2012; Yang et al.,  
178 2013; Chai et al., 2014). Moreover, slight decreases in  $PM_{2.5}$  and  $PM_{10}$  at NRCS were both evidenced by their respective  
179 difference between 2013 and 2010-2011 (Tab. 2), coincident with the results derived from the satellite data and ground  
180 monitoring in China (Ma et al., 2016; Seltenrich, 2016). For  $NO_y$ , only rough comparison was implemented due to very  
181 limited measurements executed in China. The yearly mean  $NO_y$  concentration of 63.7 ppbv in this study was slightly higher  
182 than 54.6 ppbv in Beijing (Wu et al., 2016b). It's interestingly noted that slightly higher  $NO_y$  at NRCS possibly indicated

183 more abundance of nitrogen oxides in Hangzhou. Additionally, the daytime mean concentrations were comparable with  
184 those at nighttime for PM<sub>2.5</sub> nearly in all seasons but higher for O<sub>3</sub> due to the daily variations in solar radiation and air  
185 temperature, the reverse is true for CO, NO<sub>x</sub>, and NO<sub>y</sub>.

### 186 3.2 Seasonal characteristics

187 Figure 2 shows seasonal variations of atmospheric O<sub>3</sub> (a), CO (b), NO (c), NO<sub>x</sub> (d), NO<sub>y</sub> (e), O<sub>x</sub> (f), PM<sub>2.5</sub> (g), PM<sub>10</sub> (h), and  
188 SO<sub>2</sub> (i). Ozone exhibits a distinguished seasonal variation, with a board peak in late spring and middle summer (a maximum  
189 in May and a secondary maximum in July) and a minimum in winter (November to January). Its observed behavior at NRCS  
190 is different from what has been disclosed in previous studies conducted in southern and northern China, such as a summer  
191 minimum and an autumn maximum of O<sub>3</sub> found in Hong Kong and an early summer (June) broad maximum recorded in  
192 Beijing (Ding et al., 2008; Lin et al., 2008, 2009; Xue et al., 2014; Zhang et al., 2014; Sun et al., 2016). Recently, Ding et al.  
193 (2013) presented two peaks of O<sub>3</sub> appearing in summer (July) and early autumn (September) at Xianlin site in the suburban  
194 area northeast of Nanjing (about 239 km away from NRCS station). Regarding the geographical location of Hangzhou,  
195 which is upwind of the YRD under the influence of southeasterly summer monsoon, the emissions in the YRD region and  
196 the solar radiation might be the main causes of an O<sub>3</sub> formation in summer, resulting in a different seasonal cycle of O<sub>3</sub>  
197 compared to other continent sites in the west/northwest YRD. In fact, the CO and NO<sub>y</sub> data (Fig. 2b and Fig. 2e) show that  
198 these precursors were still at fairly high levels (about 500 ppbv and 35 ppbv, respectively) in summer. The low O<sub>3</sub> level in  
199 winter, especially at night, can be attributed to the lower temperature, weaker solar radiation, and in particular the strong  
200 destruction of O<sub>3</sub> by chemical titration of NO from local emission or regional transport as discussed below (Lin et al., 2008,  
201 2009, 2011). Note that, a slight drop of O<sub>3</sub> was found in June compared with other months in summer, mainly attributing to  
202 the more frequent rainy days (23 days) and larger rainfall in June (346 mm) than those in May (15 days) and July (5 days)  
203 during summertime (Table 1).

204 For PM<sub>2.5</sub> and PM<sub>10</sub>, Fig. 2g and -2h both displayed overall well-defined seasonal variations with the maximum in winter  
205 (December) and the minimum in summer (July). In cold seasons the emission of particulate matter is normally high due to  
206 more emission of fossil fuels during heating in northern China (Zhang et al., 2009), which contributed to the enhancements  
207 of particulate matters and other tracer gases (i.e., CO and NO<sub>x</sub>) at NRCS site via long-distance transport (See discussion in  
208 Section 3.4). Furthermore, in winter temperature inversion and low mixing layer contribute to decrease particulate  
209 suspension and advection (Miao et al., 2015a). Also, dry/wet deposition should have strong seasonal variations because high  
210 precipitation favors wet-deposition and high soil humidity, and the growth of deciduous plants may also favor the dry  
211 deposition of particulate matter in warm seasons (Zhang et al., 2001). The relatively low concentrations of PM<sub>2.5</sub> and PM<sub>10</sub> in  
212 summer may be also partly due to an increased vertical mixing (i.e., a higher boundary layer height) and more convection  
213 (Ding et al., 2013; Miao et al., 2015b). PM<sub>2.5</sub> mass concentration also show strong month-to-month variations. The  
214 simultaneous drop of PM<sub>2.5</sub> and PM<sub>10</sub> concentrations together with other primary pollutants (i.e., SO<sub>2</sub>, CO and NO<sub>y</sub>) in  
215 February was mainly ascribed to the winter break of the Chinese Spring Festival, which started at the end of January and

216 lasted until mid-February. Notably, the seasonal pattern for PM was similar to  $\text{NO}_x$ , which suggested that traffic and heating  
217 emissions were important to the  $\text{PM}_{2.5}$  variation.

218 For other trace gases ( $\text{CO}$ ,  $\text{NO}_x$ ,  $\text{NO}_y$ , and  $\text{SO}_2$ ), they all revealed clear seasonal variations but also some unique month-to-  
219 month variation patterns (Fig. 2a-2f and Fig. 2i). Similar seasonal patterns among  $\text{CO}$ ,  $\text{NO}_x$ , and  $\text{SO}_2$  were generally found  
220 with pronounced minimums appearing in summer and higher levels in fall and winter. Similar reasons with particulate  
221 matters could interpret these seasonal patterns such as the variation in the boundary layer height and the long-distance  
222 transport as mentioned above. The last but not the least was photochemistry. During summer, it's most active to accelerate  
223 the transformation of primary gaseous pollutants, whereas in winter, weaker photochemical reaction cannot remove the gases  
224 as quickly as in the warmer seasons from the atmosphere.

225  $\text{NO}_y$  concentration increased at the end of autumn, with a maximum in December together with a sharp peak of  $\text{NO}$ . Time  
226 series implied that in December there was a multi-day episode of  $\text{NO}_x$  with high mixing ratios of  $\text{NO}$  and  $\text{NO}_2$  both reaching  
227 up to 100 ppbv and these days were generally correlated with northwest wind, suggesting a fresh emission from factories in  
228 the industrial zone in the northwest. The "potential ozone"  $\text{O}_x$  ( $\text{O}_3 + \text{NO}_2$ ) is usually used as an estimate of atmospheric total  
229 oxidant (Lin et al., 2008). In summer (Fig. 2f), an abnormally high level of  $\text{O}_x$  was found in winter with low  $\text{O}_3$ . The high  
230 level of  $\text{NO}_2$  in  $\text{O}_x$  was expected to be originated from the significant titration of high  $\text{NO}$  by  $\text{O}_3$  in November and December  
231 (Fig. 2a).

232 As shown in Fig. 2i,  $\text{SO}_2$  displayed a strong increase in winter but a significant drop in November. This pronounced  
233 winter peaks were mainly due to the increased coal consumption for heating as mentioned above. The drop was associated  
234 with the  $\text{PM}_{2.5}$  maximum and a relatively high RH (Fig. 2g and Table 1), suggesting a possible role of heterogeneous  
235 reactions (Ravishankara, 1997).

### 236 3.3 Inter-species correlations

237 Inter-species correlation could be normally used as an agent for acquiring some insights on their chemical formation,  
238 removal processes, and interactions. As displayed in Fig. 3 and Fig. 4, we presented scatter plots of  $\text{NO}_y$ - $\text{O}_3$ ,  $\text{NO}_y$ - $\text{PM}_{2.5}$ ,  
239  $\text{NO}_y$ - $\text{SO}_2$ ,  $\text{O}_3$ - $\text{PM}_{2.5}$ , and  $\text{NO}_y$ - $\text{CO}$  correlations based on the whole dataset, respectively, and further discriminated these  
240 correlations under typical environmental or meteorological impacts with color-coded parameters (i.e., relative humidity, air  
241 temperature, and  $\text{O}_3$  concentration). Clearly, overall negative correlation was found between  $\text{O}_3$  and  $\text{NO}_y$  during the whole  
242 period (Fig. 3a). The color data showed that negative correlation mainly appeared with data of low air temperature, implying  
243 a remarkable titration of freshly emitted  $\text{NO}$  with  $\text{O}_3$  during the cold seasons and at nighttime. In contrast, a positive  
244 correlation between  $\text{O}_3$  and  $\text{NO}_y$  dominated under high air temperature, which usually occurred in the daytime of warm  
245 seasons within a moderate level of  $\text{NO}_y$  (<150 ppbv). These findings suggested a strong local photochemical production of  
246  $\text{O}_3$  in summer, leading to its seasonal variations as illustrated in Fig. 2a.

247 As illustrated in Fig. 3b, a good positive correlation was found between  $\text{PM}_{2.5}$  and  $\text{NO}_y$ , suggesting that  $\text{PM}_{2.5}$  was highly  
248 correlated with fossil combustion at this site. Some green data in the plot show very high  $\text{NO}_y$  concentration together with



249 low  $PM_{2.5}$ , suggesting that high NO air masses during December. Fig. 3b exhibited that high RH data were very scattered but  
250 not very high  $PM_{2.5}/NO_y$ , implying that negligible interference of humidity on TEOM  $PM_{2.5}$  measurement during the study  
251 period, even under high RH condition in summer.

252  $SO_2$  and  $NO_y$  show a moderate to good correlation (See Fig. 3c). Specifically, a better correlation and higher  $SO_2/NO_y$   
253 ratio were gained from air with low humidity. Nevertheless, the point distribution was much more scattered for the humid air  
254 masses, and the ratio of  $SO_2/NO_y$  was clearly low, confirming a higher conversion of  $SO_2$  to sulfate and/or deposition in the  
255 humid condition (Khoder, 2002; Su et al., 2011). In this study, the averaged ratios of  $SO_2/NO_y$  during 18 February-30 April  
256 was lower as 0.017, compared with that previously reported at Lin'an during the same months twelve years ago (Wang et al.,  
257 2004). It was mainly owing to a remarkable reduction of  $SO_2$  emission from power plants but an increased  $NO_x$  emission  
258 associated with a huge consumption of petroleum fuels in the past decade in this region (Zhang et al., 2009).

259 A scatter plot of  $O_3$  with  $PM_{2.5}$  color-coded with air temperature was depicted in Fig. 3d. During moderate to high air  
260 temperature, a significant positive correlation was elucidated between  $O_3$  and  $PM_{2.5}$  and the reverse negative correlation was  
261 found under low temperature. The positive correlation for warm air might reflect a formation of secondary fine particulates  
262 in summer associated with high  $O_3$ , which was confirmed by our comparison of the ratio of the averaged  $PM_{2.5}$   
263 concentrations in the typical  $O_3$  exceedances events (OE) to that in nearby non- $O_3$  exceedances (NOE) events ( $PM_{2.5(OE)}/$   
264  $PM_{2.5(NOE)}$ ) with the ratios for other gaseous pollutants (Table S1 in the Supplement). The secondary particulate formation  
265 may be related to high conversion rate of  $SO_2$  and  $NO_x$  to sulfate and nitrate under a high concentration of oxidants (Khoder,  
266 2002; Sun et al., 2013). Additionally, it was also associated with the formation of secondary organic aerosols with high  $O_3$   
267 concentrations (Kamens et al., 1999; Lambe et al., 2015; Palm et al., 2017), which was primarily produced through the  
268 photo-oxidation of BVOCs (Claeys, et al., 2004; Böge et al., 2013). As inferred above, significant emission of BVOCs was  
269 speculated around NRCS in summer. Note that it's necessary to implement more detailed investigations related with  
270 chemical elements, ion, and OC/EC analysis of particulate matters. The anti-correlation for cold air might be caused by the  
271 titration effect of high NO concentration in relation to high primary  $PM_{2.5}$  in cold seasons, which was also reflected by the  
272 consistency of the seasonal variations in NO and  $PM_{2.5}$ .

273 Figure 4 shows a good positive correlation between CO and  $NO_y$  color-coded with  $O_3$  mixing ratios. For CO lower than  
274 3.2 ppmv during the whole period, an increase of  $NO_y$  generally led to lower  $O_3$  concentrations, but CO reversed. As a  
275 common origin of VOCs and CO, VOCs play a similar behavior with CO in the ozone photochemistry in the typical urban  
276 region (Atkinson, 2000; Guo et al., 2004). Our results suggested a VOCs-limited regime throughout the year in Hangzhou,  
277 consistent with the reported results in other cities of YRD region (e.g., Shanghai and Nanjing) (Geng et al., 2007; Ding et al.,  
278 2013). While, as specifically shown in Fig. 4b, atmospheric  $O_3$  (above 80 ppbv), mainly occurred in the afternoon (14:00-  
279 16:00 LT) in the summer and early autumn, exhibited increased trend with the increasing  $NO_y$  within air masses with  
280 moderated CO mixing ratio of 0.25-1.5 ppmv, and the reversed trend for CO was not expected to be significantly increased.  
281 It indicated that the transition from VOCs-limited regime to an optimum  $O_3$  production zone (even  $NO_x$ -limited regime),  
282 probably occurred at NRCS site in warmer seasons. We speculated this change was mainly attributed to the larger emission

283 of biogenic VOCs (BVOCs) compared to cold seasons. As reviewed by Calfapietra et al. (2013), the VOC-limited conditions,  
284 in which O<sub>3</sub> production is limited by a high concentration of NO<sub>x</sub>, are often observed in urban areas. However, if high  
285 BVOC emitters are common in urban areas, they could move the VOC/NO<sub>x</sub> ratio toward optimal values for O<sub>3</sub> formation,  
286 and resulted in this ratio reaching in the city centers. As depicted in Section 2.1, our study site is situated adjacent to Prince  
287 Bay Park (area, 0.8 km<sup>2</sup>) and in the northeast of West Lake famous scenic spot (area, 49 km<sup>2</sup>). For these two regions, they  
288 were both block green parks with high vegetation coverage. Moreover, the primary tree species in these two regions are  
289 Liquidambar formosana and Cinnamomum camphora, respectively, as major contributor to the emissions of isoprene and  
290 monoterpene (Chang et al., 2012), favoring the formation of O<sub>3</sub>. Air masses from Prince Bay Park and West Lake famous  
291 scenic spot were confirmed to be transported to NRCS site during warmer seasons, as illustrated in Fig. S1 and Fig. 8b. In  
292 view of the strong temperature dependence of isoprenoid emission (Guenther et al., 1995), a significantly increased emission  
293 of BVOCs was expected in warm seasons and thus it disturbed the original balance between VOCs and NO<sub>x</sub> relative to cold  
294 seasons. Our conclusion was generally in line with the contemporaneous study implemented by Li et al. (2016a) who found  
295 that VOCs-limited regime accounted for 47% of the ozone formation during the summer in Hangzhou, and the others are  
296 under NO<sub>x</sub>-limited, taking BVOCs into consideration. Recently, Li et al. (2017) also deduced the summer ozone mostly  
297 presented VOCs-limited and transition region alternately in urban Hangzhou.

### 298 **3.4 Dependences of pollutant concentrations on local emission and regional transport**

299 To overview the impact of wind on the pollutants concentrations, we draw the seasonal wind dependence maps of pollutants  
300 concentrations with wind sectors (See Fig. S2 in the Supplement for details). In total, similar seasonal patterns of wind  
301 dependence map were found between CO and PM<sub>2.5</sub>, SO<sub>2</sub>, and NO<sub>y</sub> (NO<sub>x</sub>), in good agreement with their seasonal patterns as  
302 shown in Section 3.2. For CO and PM<sub>2.5</sub>, their top 10% concentrations were generally related with all the directions  
303 throughout the year at speeds lower than 2 m s<sup>-1</sup> while bottom 10% were associated with others direction wind except north  
304 at higher wind speed. It's necessary to pay attention to the scatter points of top 10% concentrations distributed in north  
305 direction with high wind speed. With respect to the wind direction and transport, as the wind speed increases, pollutants  
306 concentrations should have been decreasing due to the more effective local dilution, thus the increase instead might indicate  
307 potential sources in these directions.

308 To address this issue and further investigate the relative contribution of local emission and regional transport, we  
309 employed the trajectory clustering and WPSCF, along the comparison with the emission inventories. The 72 h back  
310 trajectories from NRCS site were computed by using HYSPLIT model for four seasons. As shown in Fig. 9a, we obtained  
311 six clusters by the clustering algorithm for four seasons with seven dominant paths distributed in east (E), northeast (NE),  
312 north (N), northwest (NW), west (W), southwest (SW), and southeast (SE). The length of the cluster-mean trajectories  
313 indicates the transport speed of air masses. In this analysis, the long and fast moving trajectories were disaggregated into  
314 groups originating from more distant SE and SW regions during summer and NW and N regions during other seasons.  
315 Member of this cluster have extremely long transport patterns, some of them even cross over Inner Mongolia and Mongolia

316 (e.g., N and NW). Trajectories belonging to S-SW and E-SE typically followed flow patterns from South Sea and Pacific  
317 Ocean, respectively. Otherwise, some trajectories have short transport patterns, indicative of slow-moving air masses. Most  
318 of the pollution episodes within this group are probably enriched from regional and local emission sources. Such trajectories  
319 were also identified during every season in our study. For instance, the air masses associated with cluster 4 (in spring,  
320 autumn, and winter) and cluster 1 in summer were predominantly originating from local areas and the nearby provinces with  
321 significant pollution sources such as Jiangsu, Anhui, and Shanghai.

322 Table 3 summarizes the percentages of these identified trajectory clusters on seasonal basis and the corresponding mean  
323 concentrations of PM<sub>2.5</sub> and other trace gases related to each trajectory cluster. As inferred from Table 3, the clusters  
324 exhibited larger variability and season dependence: the predominant clusters were W (42.66%) in spring, SW (53.89%) in  
325 summer, NW (35.53%) in autumn, and N (54.91%) in winter, respectively. It's of interest to note that some trajectory  
326 clusters with small percentages are remarkably related with high pollutants concentrations. In summer, a few PM<sub>2.5</sub> pollution  
327 cases (only 8.42% of the summertime trajectories) with mean concentration as high as 51.5 μg m<sup>-3</sup> were related with the N  
328 trajectories travelling across well-industrialized cities cluster (i.e., Suzhou, Wuxi, and Changzhou).

329 Furthermore, we depicted the seasonal WPSCF maps (a), the corresponding zoomed maps (b), and the emissions maps (c)  
330 for PM<sub>2.5</sub>, O<sub>3</sub>, CO, NO<sub>x</sub>, and SO<sub>2</sub>, respectively, denoted with alphabets a, b, and c in the figure captions. Here we presented  
331 the results of two representative species PM<sub>2.5</sub> (Fig. 6a, -6b, and -6c) and O<sub>3</sub> (Fig. 7a, -7b) and those of the other species  
332 were included in the Supplement (Fig. S3a, -S5c). Judging from the WPSCF maps, together with their corresponding  
333 zoomed views and the calculated emissions maps, a few distinct features were summarized: (1) Local emissions were both  
334 significant for the primary pollutants such as CO (Fig. S3), NO<sub>x</sub> (Fig. S4), SO<sub>2</sub> (Fig. S5), and PM<sub>2.5</sub> (Fig. 6) on seasonal scale.  
335 For O<sub>3</sub>, local photochemistry dominated during spring, summer, and autumn (Fig. 7a, -7b) due to strong photochemical  
336 reactivity; (2) The potential sources of CO and NO<sub>x</sub> had similar patterns on spatial and seasonal scales, with higher values in  
337 the NW during spring, covering the mid-YRD regions across Anhui Province and reaching the border of Henan Province; in  
338 the NW and N during autumn and winter, covering the most area of Jiangsu Province and part of Shandong Province such as  
339 Jinan, and Zibo city; (3) the higher values for SO<sub>2</sub> were located in the Ningbo city and the coast of Yellow Sea during spring,  
340 in the southeastern region from East Sea during summer, probably due to ship emissions (Fan et al., 2016), but in the inland  
341 cities such as Shaoxing and Quzhou city of Zhejiang Province during autumn and Anhui Province during winter. In total,  
342 along with the air mass trajectories, the WPSCF maps for these primary pollutants were generally in line with their  
343 respective corresponding species' emissions (Fig. 6c, -S3c, -S4c, and -S5c). Although no seasonal patterns in emission maps  
344 were found, the emissions of these pollutants exhibited interspecies similarity and strong spatial dependence with  
345 industrialization level.

346 In terms of PM<sub>2.5</sub>, the potential sources showed distinct seasonal variations such as southeastern regions of Jiangxi  
347 Province and northwestern area of Zhejiang Province during spring and in the western city of North Korea (Pyongyang) and  
348 South Korea (Seoul) with the northeasterly air mass across Yellow Sea during summer. As illustrated in Fig. 6a and -6b, the  
349 contributions from local emission were both found to be more significant for autumn and winter than spring and summer,

350 covering all the cities in Zhejiang Province especially for the southern and southwestern part (e.g., Lishui, Jinhua, and  
351 Quzhou city). Moreover, we found the higher WPSCF values located in the middle city of Jiangsu Province in autumn and  
352 the expanded area towards the whole Jiangsu and Anhui Province and the southeast coast cities (e.g., Wenzhou, Ningbo in  
353 Zhejiang Province, Fuzhou in Fujian Province) in winter, revealing the cross-boundary transport is crucial to the pollution of  
354 particulate matters. This result has been confirmed by Yu et al. (2014) who also found such transport dominated in the  
355 Hangzhou city during the heavy haze episode (3-9 December, 2013).

356 For O<sub>3</sub>, its potential sources should be interpreted with cautions since it's not directly emitted to the atmosphere and has  
357 complicated chemistry involved with VOCs and NO<sub>x</sub>. The majority of the measured O<sub>3</sub> is probably formed by  
358 photooxidation in the vicinity of the measurement site (Fig. 7b), named as local contribution, but clear differences associated  
359 with regional transport were illustrated in Fig. 7a. In spring, high O<sub>3</sub> concentrations were connected with air masses coming  
360 from the western and southwestern region (e.g., Anhui, Jiangxi, and mid-Guangdong Province), and the northwestern area  
361 such as Jiangsu, Henan, and Shandong Province; In summer, more extensive potential sources were elucidated to be located  
362 in the eastern-southern-southwestern regions of China, covering the southern part of Zhejiang Province, southeastern cities  
363 of Jiangxi Province, almost the whole Fujian Province, and the eastern part of Guangdong Province; the mid-Zhejiang  
364 Province (e.g., Quzhou, Jinhua, and Ningbo city). A very interesting finding should be pointed out that air masses  
365 transported from the offshore area of Yellow Sea, East Sea, and South Sea, respectively on southeastern Zhejiang, Jiangsu,  
366 and Fujian Province, were also found to be highly relevant to the elevated O<sub>3</sub> at NRCS site. It was also well evidenced by  
367 seasonal and spatial distributions of O<sub>3</sub> volume mixing ratio (VMR) simulated by MOZART-4/GEOS-5 (See the Fig. S6 in  
368 the Supplement). We speculated the recirculation of pollutants by sea- and land-breeze circulations around the cities along  
369 the YRD and Hangzhou Bay which has been confirmed by Li et al. (2015, 2016b), was largely responsible for the increased  
370 concentration of O<sub>3</sub> at NRCS site. Such an increase in O<sub>3</sub> concentrations in urbanized coastal areas have been observed and  
371 modeled in a number of studies (Oh et al., 2006; Levy et al., 2008; Martins et al., 2012). Thus, our study further emphasizes  
372 the importance of local thermally induced circulation on air quality.

### 373 **3.5 Cases studies for haze (high PM<sub>2.5</sub>) and photochemical pollution (high O<sub>3</sub>) episodes**

374 To elucidate the specific causes of high PM<sub>2.5</sub> and O<sub>3</sub> episodes including the transport and local photochemical formation, we  
375 chose two typical cases for detailed interpretations and are presented here. In this study, the haze pollution episode is defined  
376 as the event that continuous days with daily averaged PM<sub>2.5</sub> concentration exceeding 75 μg m<sup>-3</sup>, which has been also used to  
377 distinguish non-haze and haze episode in other studies (Yu et al., 2014; Wu et al., 2016a). With respect to this campaign,  
378 there were two non-haze episodes (Phase I (28 Nov.-3 Dec.), II (10-12 Dec.)), and their subsequent severe haze pollution  
379 episodes (Phase III (2-9 Dec.) and IV (13-15 Dec.)) at NRCS site, respectively, as illustrated in Fig. 8. In the Phase III, it  
380 showed that high PM<sub>2.5</sub> (up to 406 μg m<sup>-3</sup>) appeared on 7 December and board PM<sub>2.5</sub> peaks (around 300 μg m<sup>-3</sup>) occurred  
381 before and after two days. Simultaneously, CO, SO<sub>2</sub>, and NO<sub>x</sub> also reached very high levels on this day, confirming that the  
382 common origin of CO and PM<sub>2.5</sub> from heating and combustion and the rapid conversion of SO<sub>2</sub> and NO<sub>x</sub> to sulfate and

383 nitrate in PM<sub>2.5</sub> in winter. But for O<sub>3</sub>, its level reached as low as 11.5 ppbv at 15:00 LT on that day, owing to the weak  
384 photochemical activity under the severe haze pollution. Along with the high NO<sub>2</sub> concentration (around 120 ppbv), it could  
385 not produce sufficient conversion oxidants (OH and HO<sub>2</sub> radicals) for the gas-phase oxidation of SO<sub>2</sub> (Poppe et al., 1993;  
386 Hua et al., 2008), while the increased relative humidity during 6-8 December possibly favored the aqueous phase oxidation  
387 of SO<sub>2</sub>.

388 Moreover, according to the results obtained from the backward trajectory cluster and WPSCF analysis during 2-9  
389 December, 2013 (Fig. S7 in the Supplement), we found an apparent contribution from the transported air mass from  
390 northwest region such as Jiangsu Province and Anhui Province. Our results were in good agreement with contemporaneous  
391 measurement in Hangzhou (Wu et al., 2016a). Subsequently, at the end of this episode significant drops of these species  
392 except O<sub>3</sub> were observed from 00:00 LT to 23:00 LT on 9 December (i.e., 189 to 41.6 μg m<sup>-3</sup> for PM<sub>2.5</sub>, 2.3 to 1.0 ppmv for  
393 CO, and 145 to 47.9 ppbv for NO<sub>x</sub>). Weather chart and wind data suggested that the region of NRCS was always controlled  
394 by a strong continental high pressure system originating from northwest before 8 December (Fig. 9a-9f), but rapidly changed  
395 to be dominated under a strong marine high pressure system coming from east at 02:00 LT on 9 December (Fig. 9g-9h),  
396 which brought clean maritime air passing over Yellow Sea and thus caused such decreases in these pollutants. However, it  
397 quickly turned back to be controlled under a continental high pressure system described above, carrying pollutants from the  
398 city clusters to the NRCS site. It could account for the accumulations of these species during the intermediate period (Phase  
399 II). For the subsequent Phase IV with high PM<sub>2.5</sub> episode it was also found to be governed by a stagnant high pressure over  
400 YRD region (Fig. S8).

401 For the photochemical pollution events, we selected three cases with O<sub>3</sub> exceedances (74.6 ppbv) during May-August  
402 according to Grade II standard of CAAQS. As displayed in Fig. 10, they were the Phase I (28-30 May and 20-22 June) with  
403 rapid buildup and decrease of O<sub>3</sub> within 3 days, Phase II (9-12 July) representing a distinct accumulation process of O<sub>3</sub>  
404 exceedances, and the Phase III (1-3 May, 20-22 May, and 9-11 August) with high O<sub>3</sub> levels within three consecutive days.  
405 For 28 May in the Phase I, weather chart suggested that a strong anticlockwise cyclone located over YRD. In this case, the  
406 cyclone (i.e., low pressure) caused favoring conditions, e.g., cloudy weather and high wind velocities, for pollution diffusion.  
407 Then, a strong clockwise anticyclone from northwest, sweeping over cities cluster (i.e., Nanjing and Shanghai), rapidly  
408 moved adjacent to NRCS site on 29 May. It carried the primary pollutants such as CO, SO<sub>2</sub>, NO<sub>x</sub> from these megacities and  
409 secondary products (i.e., O<sub>3</sub> and some NO<sub>z</sub>) were further produced via complex photochemical reactions under such synoptic  
410 conditions. As orange shaded area shown in Fig. 10, the hourly maximums of O<sub>3</sub> and PM<sub>2.5</sub> were observed as high as 141.2  
411 ppbv and 135.8 μg m<sup>-3</sup> at 13:00 LT on 29 May. Following this day, the cyclone again dominated this region and caused  
412 sudden decreased in atmospheric pollutants. Also, similar case was found during 20-22 June under such changes in synoptic  
413 weather. For Phase II (9-12 July), a typical accumulation process was observed with the daily maximums of atmospheric  
414 pollutants increasing from 90.4 to 142.9 ppbv for O<sub>3</sub>, 77.6 to 95.3 μg m<sup>-3</sup> for PM<sub>2.5</sub>, and 80.2 to 125.2 ppbv for NO<sub>y</sub>,  
415 respectively. The examination of day-to-day 925-hPa synoptic chart derived from NECP reanalysis suggested that high  
416 pressure system governed over YRD during 9-11 July, with southwesterly prevailing wind. The air masses recorded at this

417 site mainly came from the most polluted city clusters in the southwest (e.g. Zhejiang, Jiangxi, and Fujian Province).  
418 Meanwhile, the stagnant synoptic condition (i.e., low wind speed) favored the accumulation of primary pollutants such as  
419 CO and NO<sub>x</sub>. For secondary pollutants O<sub>3</sub> and PM<sub>2.5</sub>, they were also rapidly formed via photochemical oxidation and further  
420 accumulated under such synoptic condition, together with continuous high-temperature (daily mean around 33 °C). On 12  
421 July, a typhoon (No. 7 Typhoon Soulik) moved to a location a few hundred kilometers away from NRCS site, bringing  
422 southeasterly maritime air over YRD. Daily maximum O<sub>3</sub> reached at 142.8 ppbv at 12:00 LT even with low concentration of  
423 precursors (i.e., 0.48 ppmv for CO and 16.0 ppbv for NO<sub>x</sub>), suggesting high photochemical production efficiency of O<sub>3</sub> in  
424 this region in summer. This phenomenon has been also found in the multi-day episode of high O<sub>3</sub> in Nanjing during 20-21  
425 July, 2011 (Ding et al., 2013). In this phase, PM<sub>2.5</sub> mass concentration showed very good correlation ( $R = 0.79$ ,  $p < 0.001$ )  
426 with O<sub>3</sub> during the daytime (09:00-17:00 LT), possibly indicating a common origin of BVOCs due to the significant  
427 vegetation emission as discussed above, in addition to high biomass production in the southern part of the YRD (Ding et al.,  
428 2013). For Phase III (1-3 May, 20-22 May, and 9-11 August), there were most sunny days with low wind speed and  
429 moderate/high air temperature which were both beneficial factors for photochemical formation of O<sub>3</sub>, together with sufficient  
430 precursors (NO<sub>x</sub> and VOCs) in the summer and early autumn over YRD. For 1-3 May and 20-22 May, daily maximum T  
431 were moderate (around 25 °C versus 31 °C), while the daily maximums NO<sub>x</sub> reached as high as 43-95 ppbv and 50-90 ppbv,  
432 respectively, which both favoring the photochemical formation to produce the continuous high O<sub>3</sub> concentrations (daily  
433 maximums: 96-133 ppbv via 104-133 ppbv). The reverse case is also true during 9-11 August, on which the daily maximum  
434 T and NO<sub>x</sub> ranged from 40.6-41.4 °C and 33-44 ppbv, respectively, resulting in producing continuously high O<sub>3</sub> from 98.8  
435 ppbv to 130.5 ppbv.

### 436 **3.6 Photochemical age and ozone production efficiency during photochemical pollution and haze period**

437 Photochemical age is often used to express the extent of photochemistry, which can be estimated using some indicator such  
438 as NO<sub>x</sub>/NO<sub>y</sub> (Carpenter et al., 2000; Lin et al., 2008, 2009, 2011; Parrish et al., 1992). Air masses with fresh emissions have  
439 NO<sub>x</sub>/NO<sub>y</sub> close to 1, while lower NO<sub>x</sub>/NO<sub>y</sub> ratio for the photochemical aged air masses. In this study, for the haze events as  
440 mentioned above, the average and maximum NO<sub>x</sub>/NO<sub>y</sub> ratios were as high as 0.80 and 0.99, respectively, indicating that  
441 photochemical conversion of NO<sub>x</sub> is not absent but fairly slow. It was well consistent with the largely weaken  
442 photochemistry due to the low intensity of UV radiation in winter. In contrast, during the photochemical pollution period,  
443 they were low as 0.53 and 0.14 for the average and minimum ratio. The simultaneous measurements of atmospheric O<sub>3</sub>, NO<sub>x</sub>,  
444 and NO<sub>y</sub> can provide an insight into calculating the ozone production efficiency (OPE) for different seasons. From the data  
445 of O<sub>x</sub> and NO<sub>z</sub>, the ratio of  $\Delta(O_x)/\Delta(NO_z)$  can be calculated as a kind of observation-based OPE (Trainer et al., 1993; Sillman,  
446 2000; Kleinman et al., 2002; Lin et al., 2011;). In this study, the mean values of NO<sub>z</sub> and O<sub>x</sub> between 07:00-15:00 LT, were  
447 used to calculate the OPE values through the linear regressions. In addition, these data were also confined to the sunny days  
448 and the wind speed below 3 m s<sup>-1</sup>, reflecting the local photochemistry as possible. The OPE value during the photochemical  
449 pollution period (SOPE) as mentioned above was 1.99, generally within the reported range of 1-5 in the PRD cities, but

450 lower than 3.9-9.7 in summer Beijing (Chou et al., 2009; Ge et al., 2012). Meanwhile, the OPE value of 0.77 during the haze  
451 period (HPOE) was also comparable with the reported value of 1.1 in winter in Beijing (Lin et al., 2011). The smaller winter  
452 OPE value in Hangzhou might be ascribed to the weaker photochemistry and higher NO<sub>x</sub> concentration. At high NO<sub>x</sub> level,  
453 OPE tends to decrease with the increased NO<sub>x</sub> concentration (Ge et al., 2010; Lin et al., 2011). In Hangzhou, the NO<sub>x</sub> level is  
454 frequently higher than needed for producing photochemical O<sub>3</sub>, and excessive NO<sub>x</sub> causes net O<sub>3</sub> loss rather than  
455 accumulation. In this study, 75% of daily OPE values were negative, for which two factors could be accounted. To some extent,  
456 due to the geographical location and unique climate characteristic for Hangzhou as depicted above, the interference of  
457 unbeneficial meteorological condition existed in the formation of local O<sub>3</sub> deriving from photochemistry, i.e., strong wind,  
458 frequent rainy days. The other one is because of the consumption of O<sub>3</sub> by excessive NO<sub>x</sub>, which was also well confirmed by  
459 the conclusion that Hangzhou was mostly in the VOCs-limited regime as discussed in Section 3.2. Such circumstance was  
460 also observed at the rural site Gucheng in the NCP and in Beijing urban area (Lin et al., 2009, 2011). Taking the average of  
461 SOPE of 1.99 and the average daytime increment of NO<sub>z</sub> (ca. 20 ppbv), we estimated an average photochemical O<sub>3</sub>  
462 production of about 39.8 ppbv during photochemical pollution period. In contrast, the lower average photochemical O<sub>3</sub>  
463 production was estimated to be 10.78 ppbv during haze period based on HOPE, which might act as a significant source for  
464 surface O<sub>3</sub> in winter in Hangzhou.

#### 465 **4 Conclusions**

466 In this study, we presented an overview of one year measurements of trace gases (O<sub>3</sub>, CO, NO<sub>x</sub>, NO<sub>y</sub>, and SO<sub>2</sub>) and  
467 particulate matters (PM<sub>2.5</sub> and PM<sub>10</sub>) at National Reference Climatological Station in Hangzhou. The characteristics and  
468 cause of these chemicals were investigated by their seasonal characteristics, along the comparison with the previous results  
469 in other regions in China, interspecies correlations, and the concentration dependence on local emission and regional  
470 transport. Specific photochemical pollution and haze case were studied in detail based on discussing the physical process and  
471 photochemical formation (ozone production efficiency). The main findings and conclusions are summarized below:

472 a) Within one year study period, there were 38 days of O<sub>3</sub> exceedances and 62 days of PM<sub>2.5</sub> exceedances of the National  
473 Ambient Air Quality Standards in China at the site, suggesting heavy air pollution in this region. In general, the  
474 concentration levels of these chemicals were consistent with those observed by other contemporaneous measurements in  
475 Hangzhou and the other cities in YRD, but lower than those in NCP. Distinct seasonal characteristics were found with a  
476 board peak in late spring and middle summer and a minimum in winter for O<sub>3</sub>, while with maximum in winter and minimum  
477 in summer for PM<sub>2.5</sub>.

478 b) A positive O<sub>3</sub>-NO<sub>y</sub> correlation was found for air masses with high air temperature in summer, suggesting a strong local  
479 photochemical production of O<sub>3</sub>. In addition, correlation analysis shows an important conversion of SO<sub>2</sub> to sulfate and NO<sub>x</sub>  
480 to nitrate and/or deposition in the humid condition. CO-NO<sub>y</sub>-O<sub>3</sub> correlation suggested a VOC-limited regime for the overall  
481 study period but moved toward an optimum O<sub>3</sub> production zone during warm seasons. The positive correlation between O<sub>3</sub>  
482 and PM<sub>2.5</sub> under high air temperature indicated a formation of secondary fine particulates in warm seasons, respectively.

483 c) The results from the emission inventories of the primary pollutants such as PM<sub>2.5</sub>, CO, NO<sub>x</sub>, and SO<sub>2</sub> demonstrated that  
484 local emissions were both significant for these species but without distinct seasonal variations. The major potential sources  
485 of PM<sub>2.5</sub> were located in the regions of southwesterly in spring, northwesterly and northeasterly in summer, and  
486 northwesterly (the whole Jiangsu Province and Anhui Province) in autumn and winter, respectively. For CO and NO<sub>x</sub>, they  
487 showed similar patterns with northwestern regions covering the mid-YRD regions and Anhui Province during spring and in  
488 the northwestern and northern regions including Jiangsu Province and part of Shandong Province during autumn and winter.  
489 The distinct seasonal variation in SO<sub>2</sub> potential might be from southwestern and eastern region during spring and summer  
490 but northwestern during autumn and winter. Air masses transported from the offshore area of Yellow Sea, East Sea, and  
491 South Sea, respectively on southeastern Zhejiang, Jiangsu, and Fujian Province, were also found to be highly relevant to the  
492 elevated O<sub>3</sub> at NRCS site, probably due to the recirculation of pollutants by sea- and land-breeze circulations around the  
493 cities along the YRD and Hangzhou Bay. This finding further emphasizes the importance of urban-induced circulation on air  
494 quality.

495 d) Case studies for photochemical pollution and haze episodes both suggest the combined importance of local atmospheric  
496 photochemistry and synoptic weather during the accumulation (related with anticyclones) and dilution process (related with  
497 cyclones) of these episodes. The average photochemical O<sub>3</sub> productions were estimated to be 39.8 and 10.78 ppbv during  
498 photochemical pollution and haze period, respectively, indicating local photochemistry might act as a significant source for  
499 surface O<sub>3</sub> in winter in Hangzhou.

500 Our study further completes a picture of air pollution in the YRD, interprets the physical and photochemical processes  
501 during haze and photochemical pollution episodes, and explores the seasonal and spatial variations in the potential sources of  
502 these pollutants. Moreover, this work suggests the cross-region control measures are crucial to improve air quality in the  
503 YRD region, and further emphasizes the importance of local thermally induced circulation on air quality.

504

505 **Acknowledgement.** This study is financially supported by National Key Research and Development Program of China  
506 (2016YFC0202300), National Natural Science Foundation of China (41775127, 41505108, and ), and Shanghai Key  
507 Laboratory of Meteorology and Health (QXJK201501). The authors are especially grateful to Dr. Miao Yucong for the  
508 technical supports in drawing a part of figures and discussions.

## 509 **References**

510 Atkinson, R.: Atmospheric chemistry of VOCs and NO<sub>x</sub>, *Atmos. Environ.*, 34, 2063-2101, 2000.

511 Böge, O., Mutzel, A., Linuma, Y., Yli-Pirilä, P., Kahnt, A., Joutsensaari, J., and Herrmann, H.: Gas-phase products and  
512 secondary organic aerosol formation from the ozonolysis and photooxidation of myrcene, *Atmos. Environ.*, 79, 553-560,  
513 2013.



514 Calfapietra, C., Fares, S., Manes, F., Morani, A., Sgrign, G., and Loreto, F.: Role of biogenic volatile organic compounds  
515 (BVOC) emitted by urban trees on ozone concentration in cities: A review, *Environ. Poll.*, 183, 71-80, 2013.

516 Cao, J., Shen, Z., Chow, J. C., Qi, G., and Watson, J. G.: Seasonal variations and sources of mass and chemical composition  
517 for PM<sub>10</sub> aerosol in Hangzhou, China, *Particuology*, 7, 161-168, 2009.

518 Carpenter, L. J., Green, T. J., Mills, G. P., Bauguitte, S., Penkett, S. A., Zanis, P., Schuepbach, E., Schmidbauer, N., Monks,  
519 P. S., and Zellweger, C.: Oxidized nitrogen and ozone production efficiencies in the springtime free troposphere over  
520 the Alps, *J. Geophys. Res.*, 105, 14547-14559, 2000.

521 Chai, F. H., Gao, J., Chen, Z. X., Wang, S. L., Zhang, Y. C., Zhang, J. Q., Zhang, H. F., Yun, Y. R., and Ren, C.: Spatial and  
522 temporal variation of particulate matter and gaseous pollutants in 26 cities in China, *J. Environ. Sci.*, 26, 75-82, 2014.

523 Chang, J., Ren, Y., Shi, Y., Zhu, Y. M., Ge, Y., Hong, S. M., Jiao, L., Lin, F. M., Peng, C. H., Mochizuki, T., Tani, A., Mu,  
524 Y., and Fu, C. X.: An inventory of biogenic volatile organic compounds for a subtropical urban-rural complex, *Atmos.*  
525 *Environ.*, 56, 115-123, 2012.

526 Chen, T., He, J., Lu, X., She, J., and Guan, Z.: Spatial and temporal variations of PM<sub>2.5</sub> and its relation to meteorological  
527 factors in the urban area of Nanjing, China, *Int. J. Environ. Res. Pub. Heal.*, 13, 921, 2016.

528 Cheng, Y. F., Zheng, G. J., Wei, C., Mu, Q., Zheng, B., Wang, Z. B., Gao, M., Zhang, Q., He, K. B., Carmichael, G., Pöschl,  
529 U., and Su, H.: Reactive nitrogen chemistry in aerosol water as a source of sulfate during haze events in China, *Sci.*  
530 *Adv.*, 2, 12, 1-11, 2016.

531 Chou, C. K., Tsai, C. Y., Shiu, C. J., Liu, S. C., and Zhu, T.: Measurement of NO<sub>y</sub> during campaign of air quality research in  
532 Beijing 2006 (CAREBeijing-2006): implications for the ozone production efficiency of NO<sub>x</sub>, *J. Geophys. Res.*, 114, 1,  
533 328-334, 2009.

534 Chow, J. C. and Watson, J. G.: Review of PM<sub>2.5</sub> and PM<sub>10</sub> apportionment for fossil fuel combustion and other sources by the  
535 chemical mass balance receptor model, *Energy Fuels*, 16, 2, 222-260, 2002.

536 Claeys, M., Graham, B., Vas, G., Wang, W., Vermeylen, R., Pashynska, V., Cafmeyer, J., Guyon, P., Andreae, M. O.,  
537 Artaxo, P., and Maenhaut, W.: Formation of secondary organic aerosols through photooxidation of isoprene, *Science*,  
538 303, 5661, 1173-1176, 2004.

539 Dickerson, R. R., Kondragunta, S., Stenchikov, G., Civerolo, K. L., Doddridge, B. G., and Holben, B. N.: The Impact of  
540 aerosols on solar ultraviolet radiation and photochemical pollution, *Science*, 278, 5339, 827-830, 1997.

541 Ding, A. J., Wang, T., Thouret, V., Cammas, J.-P., and Nédélec, P.: Tropospheric ozone climatology over Beijing: analysis  
542 of aircraft data from the MOZAIC program, *Atmos. Chem. Phys.*, 8, 1-13, 2008.

543 Ding, A. J., Fu, C. B., Yang, X. Q., Sun, J. N., Zheng, L. F., Xie, Y. N., Herrmann, E., Nie, W., Petäjä, T., Kerminen, V. M.,  
544 and Kulmala, M.: Ozone and fine particulate in the western Yangtze River Delta: an overview of 1 yr data at the  
545 SORPES station, *Atmos. Chem. Phys.*, 13, 5813-5830, 2013.

546 Fan, Q., Zhang, Y., Ma, W., Ma, H., Feng, J., Yu, Q., Yang, X., Ng, S.K.W., Fu, Q., and Chen, L.: Spatial and seasonal  
547 dynamics of ship emissions over the Yangtze River Delta and East China Sea and their potential environmental  
548 influence, *Environ. Sci. Technol.*, 50, 1322-1329, 2016.

549 Feng, Z. Z., Sun, J. S., Wan, W. X., Hu, E. Z., and Calatayud, V.: Evidence of widespread ozone-induced visible injury on  
550 plants in Beijing, China, *Environ. Pollut.*, 193, 296-301, 2014.

551 Ge, B. Z., Xu, X. B., Lin, W. L., and Wang, Y.: Observational study of ozone production efficiency at the Shangdianzi  
552 regional background station, *Environ. Sci.*, 31, 7, 1444-1450, 2010 (In Chinese with English abstract).

553 Ge, B. Z., Xu, X. B., Lin, W. L., Li, J., and Wang, Z. F.: Impact of the regional transport of urban Beijing pollutants on  
554 downwind areas in summer: ozone production efficiency analysis, *Tellus*, 64, 17348, 2012.

555 Geng, F. H., Zhao, C. S., Tang, X., Lu, G. L., and Tie, X. X.: Analysis of ozone and VOCs measured in Shanghai: A case study,  
556 *Atmos. Environ.*, 41, 989-1001, 2007.

557 Guenther, A., Hewitt, C. N., Erickson, D., Fall, R., Geron, C., Graedel, T., Harley, P., Klinger, L., Lerdau, M., McKay, W.  
558 A., Pierce, T., Scholes, B., Steinbrecher, R., Tallamraju, R., Taylor, J., and Zimmerman, P. L.: A global model of  
559 natural volatile organic compound emissions, *J. Geophys. Res.*, 100, 8873-8892, 1995.

560 Guo, H., Wang, T., Simpson, I. J., Blake, D. R., Yu, X. M., Kwok, Y. H., and Li, Y. S.: Source contributions to ambient  
561 VOCs and CO at a rural site in eastern China, 38(27), 4551-4560, 2004.

562 He, K. B., Huo, H., and Zhang, Q.: Urban air pollution in China: current status, characteristics, and progress, *Annu. Rev.*  
563 *Energ. Env.*, 27, 397-431, 2002.

564 Hsu, Y.K., Holsen, T. M., and Hopke, P. K.: Comparison of hybrid receptor models to locate PCB sources in Chicago,  
565 *Atmos. Environ.*, 37, 545-562, 2003.

566 Hua, W., Chen, Z. M., Jie, C. Y., Kondo, Y., Hofzumahaus, A., Takegawa, N., Chang, C. C., Lu, K. D., Miyazaki, Y., Kita,  
567 K., Wang, H. L., Zhang, Y. H., and Hu, M.: Atmospheric hydrogen peroxide and organic hydroperoxides during  
568 PRIDE-PRD'06, China: their concentration, formation mechanism and contribution to secondary aerosols, *Atmos.*  
569 *Chem. Phys.*, 8, 6755-6773, 2008.

570 Huang, Y., Shen, H. Z., Chen, H., Wang, R., Zhang, Y. Y., Su, S., Chen, Y. C., Lin, N., Zhao, S. J., Zhong, Q. R., Wang, X.  
571 L., Liu, J. F., Li, B. G., Liu, W. X., and Tao, S.: Quantification of global primary emissions of PM<sub>2.5</sub>, PM<sub>10</sub>, and TSP  
572 from combustion and industrial process sources, *Environ. Sci. Technol.*, 48, 13834-13843, 2014.

573 IPCC, Summary for Policymakers. In *Climate Change 2007: The Physical Science Basis. Contribution of Working Group I*  
574 *to the Fourth Assessment Report of the Intergovernmental Panel on Climate Change*; Solomon, S., Qin, D., Manning,  
575 M., Chen, Z., Marquis, M., Averyt, K. B., Tignor, M., Miller, H. L., Eds.; Cambridge University Press: Cambridge,  
576 United Kingdom and New York, NY, USA, 2007.

577 Jansen, R. C., Shi, Y., Chen, J. M., Hu, Y. J., Xu, C., Hong, S. M., Jiao, L., and Zhang, M.: Using hourly measurements to  
578 explore the role of secondary inorganic aerosol in PM<sub>2.5</sub> during haze and fog in Hangzhou, China. *Adv. Atmos. Sci.*, 31,  
579 1427-1434, 2014.

580 Kamens, R., Jang, M., Chien, C.J., and Leach, K.: Aerosol formation from reaction of  $\alpha$ -pinene and ozone using a gas-phase  
581 kinetics-aerosol partitioning model, *Environ. Sci. Technol.*, 33, 1430-1438, 1999.

582 Kang, H., Zhu, B., Su, J., Wang, H., Zhang, Q., and Wang, F.: Analysis of a long-lasting haze episode in Nanjing, China,  
583 *Atmos. Res.*, 120-121, 78-87, 2013.

584 Khoder, M. I.: Atmospheric conversion of sulfur dioxide to particulate sulfate and nitrogen dioxide to particulate nitrate and  
585 gaseous nitric acid in an urban area, *Chemosphere*, 49, 675-684, 2002.

586 Kleinman, L., Daum, P. H., Lee, Y.-N., Nunnermacker, L. J., Springston, S. R., Weinstein-Lloyd, J., and Rudolph, J.: Ozone  
587 production efficiency in an urban area, *J. Geophys. Res.*, 107, 4733, 2002.

588 Lambe, A. T., Chhabra, P. S., Onasch, T. B., Brune, W. H., Hunter, J. F., Kroll, J. H., Cummings, M. J., Brogan, J. F.,  
589 Parmar, Y., Worsnop, D. R., Kolb, C. E., and Davidovits, P.: Effect of oxidant concentration, exposure time, and seed  
590 particulates on secondary organic aerosol chemical composition and yield, *Atmos. Chem. Phys.*, 15, 3063-3075, 2015.

591 Levy, I., Dayan, U., and Mahrer, Y.: A five-year study of coastal recirculation and its effect on air pollutants over the east  
592 Mediterranean region, *J. Geophys. Res.*, 113, D16121, 2008.

593 Li, M. M., Mao, Z. C., Song, Y., Liu, M. X., and Huang, X.: Impact of the decadal urbanization on thermally induced  
594 circulations in eastern China, *J. Appl. Meteorol. Clim.*, 54, 259-282, 2015.

595 Li, L., An, J. Y., Shi, Y. Y., Zhou, M., Yan, R. S., Huang, C., Wang, H. L., Lou, S. R., Wang, Q., Lu, Q., and Wu, J.: Source  
596 apportionment of surface ozone in the Yangtze River Delta, China in the summer of 2013, *Atmos. Environ.*, 144, 194-  
597 207, 2016a.

598 Li, M. M., Song, Y., Mao, Z. C., Liu, M. X., and Huang, X.: Impact of thermal circulations induced by urbanization on  
599 ozone formation in the Pearl River Delta, China, *Atmos. Environ.*, 127, 382-392, 2016b.

600 Li, K. W., Chen, L. H., Ying, F., White, S. J., Jang, C., Wu, X. C., Gao, X., Hong, S. M., Shen, J. D., Azzi, M., and Cen, K.  
601 F.: Meteorological and chemical impacts on ozone formation : A case study in Hangzhou, China, *Atmos. Res.*, doi:  
602 10.1016/j.atmosres.2017.06.003, 2017.

603 Lin, W. L., Xu, X. B., Zhang, X. C., and Tang, J.: Contributions of pollutants from North China Plain to surface ozone at the  
604 Shangdianzi GAW Station, *Atmos. Chem. Phys.*, 8, 5889-5898, 2008.

605 Lin, W. L., Xu, X. B., Ge, B. Z., and Zhang, X. C.: Characteristics of gaseous pollutants at Gucheng, a rural site southwest  
606 of Beijing, *J. Geophys. Res.*, 114, 4723-4734, 2009.

607 Lin, W. L., Xu, X. B., Ge, B. Z., and Liu, X.: Gaseous pollutants in Beijing urban area during the heating period 2007-2008:  
608 variability, sources, meteorological, and chemical impacts, *Atmos. Chem. Phys.*, 11, 8157-8170, 2011.

609 Liu, G., Li, J. H., Wu, D., and Xu, H.: Chemical composition and source apportionment of the ambient PM<sub>2.5</sub> in Hangzhou,  
610 China, *Particuology*, 18, 135-143, 2015.

611 Liu, T., Li, T. T., Zhang, Y. H., Xu, Y. J., Lao, X. Q., Rutherford, S., Chu, C., and Luo, Y.: The short-term effect of ambient  
612 ozone on mortality is modified by temperature in Guangzhou, China, *Atmos. Environ.*, 76, 59-67, 2013.

613 Logan, J. A.: Tropospheric ozone: Seasonal behavior, trends, and anthropogenic influence. *J. Geophys. Res.*, 90, 10463-  
614 10482, 1985.

615 Luo, C., St. John, J. C., Zhou, X. J., Lam, K. S., Wang, T., and Chameides, W. L.: A nonurban ozone air pollution episode  
616 over eastern China: observations and model simulations, *J. Geophys. Res.*, 105, 1889-1908, 2000.

617 Ma, Z. W., Hu, X. F., Sayer, A. M., Levy, R., Zhang, Q., Xue, Y. G., Tong, S. L., Bi, J., Huang, L., and Liu, Y.: Satellite-  
618 based spatiotemporal trends in PM<sub>2.5</sub> concentrations: China, 2004-2013, *Environ. Health Persp.*, 124, 184-192, 2016.

619 Martins, D. K., Stauffer, R. M., Thompson, A. M., Knepp, T. N., and Pippin, M.: Surface ozone at a coastal suburban site in  
620 2009 and 2010: relationships to chemical and meteorological processes, *J. Geophys. Res.*, 117, D5, 5306, 2012.

621 Meagher, J. F., Stockburger, L., Bailey, E. M., and Huff, O.: The oxidation of sulfur dioxide to sulfate aerosols in the plume  
622 of a coal-fired power plant, *Atmos. Environ.*, 12, 11, 2197-2203, 1978.

623 Mercado, L. M. Bellouin, N. Sitch, S. Boucher, O. Huntingford, C. Wild, M. and Cox, P. M.: Impact of changes in diffuse  
624 radiation on the global land carbon sink, *Nature*, 458, 7241, 1014-1017, 2009.

625 Miao, Y. C., Liu, S. H., Zheng, Y. J., Wang, S., Liu, Z. X., and Zhang, B. H.: Numerical study of the effects of planetary  
626 boundary layer structure on the pollutant dispersion within built-up areas, *J. Environ. Sci.*, 32, 168-179, 2015a.

627 Miao, Y. C., Hu, X. M., Liu, S. H., Qian, T., Xue, M., Zheng, Y., and Wang, S.: Seasonal variation of local atmospheric  
628 circulations and boundary layer structure in the Beijing-Tianjin-Hebei region and implications for air quality, *J. Adv.  
629 Model. Earth Syst.*, 7, 1, 1-25, 2015b.

630 Miao, Y. C., Guo, J. P., Liu, S. H., Liu, H., Zhang, G., Yan, Y., and He, J.: Relay transport of aerosols to Beijing-Tian-Hebei  
631 region by multi-scale atmospheric circulations, *Atmos. Environ.*, 165, 35-45, 2017a.

632 Miao, Y. C., Guo, J. P., Liu, S. H., Liu, H., Li, Z. Q., Zhang, W. C., and Zhai, P. M.: Classification of summertime synoptic  
633 patterns in Beijing and their associations with boundary structure affecting aerosol pollution, *Atmos. Chem. Phys.*, 17,  
634 3097-3110, 2017b.

635 Ministry of Environmental Protection of China (MEP), Ambient air quality standards (GB 3095-2012), 12 pp., China  
636 Environmental Science Press, Beijing, 2012 (in Chinese).

637 Oh, I. B., Kim, Y. K., Lee, H. W., and Kim, C. H.: An observational and numerical study of the effects of the late sea breeze  
638 on ozone distributions in the Busan metropolitan area, Korea, *Atmos. Environ.*, 40, 1284-1298, 2006.

639 Palm, B. B., Campuzano-Jost, P., Day, D. A., Ortega, A. M., Fry, J. L., Brown, S. S., Zarzana, K. J., Dube, W., Wagner, N.  
640 L., Draper, D. C., Kaser, L., Jud, W., Karl, T., Hansel, A., Gutiérrez-Montes, C., and Jimenez, J. L.: Secondary organic  
641 aerosol formation from in situ OH, O<sub>3</sub>, and NO<sub>3</sub> oxidation of ambient forest air in an oxidation flow reactor, *Atmos.  
642 Chem. Phys.*, 17, 5331-5354, 2017.

643 Parrish, D. D., Hahn, C. J., Williams, E. J., Borton, R. B., Fehsenfeld, F. C., Singh, H. B., Shetter, J. D., Gandrud, B. W., and  
644 Ridley, B. A.: Indications of photochemical histories of Pacific air masses from measurements of atmospheric trace  
645 species at Point Arena, California, *J. Geophys. Res.*, 97, 15883-15901, 1992.

646 Polissar, A.V., Hopke, P.K., Paatero, P., Kaufmann, Y.J., Hall, D.K., Bodhaine, B.A., Dutton, E.G. and Harris, J.M.: The  
647 aerosol at Barrow, Alaska: long-term trends and source locations. *Atmos. Environ.*, 33, 2441-2458, 1999.

648 Pope, C. and Dockery, D.: Epidemiology of particulate effects. In *Air pollution and health*; Holgate, S. T., Koren, H. S.,  
649 Samet, J. M., Maynard, R. L., Eds.; Academic Press: San Diego; 673-705, 1999.

650 Poppe, D., Wallasch, M., and Zimmermann, J.: The dependence of the concentration of OH on its precursors under  
651 moderately polluted conditions: a model study, *J. Atmos. Chem.*, 16, 61-78, 1993.

652 Qi, B., Du, R., Yu, Z., Zhou, B., and Yuan, X.: Characteristics of atmospheric fine particulates concentrations in Hangzhou  
653 region, *Environ. Chem.*, 34, 77-82, 2015.

654 Qi, H. X., Lin, W. L., Xu, X. B., Yu, X. M., and Ma, Q. L.: Significant downward trend of SO<sub>2</sub> observed from 2005 to 2010  
655 at a background station in the Yangtze Delta region, China, *Sci. China Chem.*, 55, 7, 1451-1458, 2012.

656 Ravishankara, A. R.: Heterogeneous and multiphase chemistry in the troposphere, *Science*, 276, 1058-1065, 1997.

657 Roelofs, G. J. and Lelieveld, J.: Model study of the influence of cross-tropopause O<sub>3</sub> transports on tropospheric O<sub>3</sub> levels,  
658 *Tellus B*, 49, 38-55, 1997.

659 Saxena, P. and Seigneur, C.: On the oxidation of SO<sub>2</sub> to sulfate in atmospheric aerosols, *Atmos. Environ.*, 21, 4, 807-812,  
660 1987.

661 Seinfeld, J. H., Carmichael, G. R., Arimoto, R., Conant, W. C., Brechtel, F. J., Bates, T. S., Cahill, T. A., Clarke, A. D.,  
662 Doherty, S. J., Flatau, P. J., Huebert, B. J., Kim, J., Markowicz, K. M., Quinn, P. K., Russell, L. M., Russell, P. B.,  
663 Shimizu, A., Shinozuka, Y., Song, C. H., Tang, Y. H., Uno, I., Vogelmann, A. M., Weber, R. J., Woo, J. H., and Zhang,  
664 X. Y.: ACE-ASIA - Regional climatic and atmospheric chemical effects of Asian dust and pollution. *Bull. Am.*  
665 *Meteorol. Soc.*, 85, 3, 367-380, 2004.

666 Seinfeld, J. H. and Pandis, S. N.: *Atmospheric Chemistry and Physics: From Air Pollution to Climate Change*, 2nd ed., John  
667 Wiley & Sons: New York, USA, 57-58 and 381-383, 2006

668 Seltenrich, N.: A clearer picture of China's air using satellite data and ground monitoring to estimate PM<sub>2.5</sub> over time,  
669 *Environ. Health Persp.*, 124, A38, 2016.

670 Shao, M., Tang, X. Y., Zhang, Y. H., and Li, W. J.: City clusters in China: air and surface water pollution, *Front. Ecol.*  
671 *Environ.*, 4, 7, 353-361, 2006.

672 Sillman, S.: Ozone production efficiency and loss of NO<sub>x</sub> in power plant plumes: photochemical model and interpretation of  
673 measurements in Tennessee, *J. Geophys. Res.*, 105, 9189-9202, 2000.

674 Streets, D. G., Fu, J. S., Jang, C. J., Hao, J. M., He, K. B., Tang, X. Y., Zhang, Y. H., Wang, Z. F., and Li, Z. P.: Air quality  
675 during the 2008 Beijing Olympic Games, *Atmos. Environ.*, 41, 480-492, 2007.

676 Su, S., Li, B. G., Cui, S. Y., and Tao, S.: Sulfur dioxide emissions from combustion in China: from 1990 to 2007, *Environ.*  
677 *Sci. Technol.*, 45, 8403-8410, 2011.

678 Sun, L., Xue, L. K., Wang, T., Gao, J., Ding, A. J., Cooper, O. R., Lin, M. Y., Xu, P. J., Wang, Z., Wang, X. F., Wen, L.,  
679 Zhu, Y. H., Chen, T. S., Yang, L. X., Wang, Y., Chen, J. M., and Wang, W. X.: Significant increase of summertime  
680 ozone at Mount Tai in Central Eastern China, *Atmos. Chem. Phys.*, 16, 10637-10650, 2016.

681 Sun, G., Yao, L., Jiao, L., Shi, Y., Zhang, Q., Tao, M., Shan, G., and He, Y.: Characterizing PM<sub>2.5</sub> pollution of a subtropical  
682 metropolitan area in China, *Atmos. Climate. Sci.*, 3, 11, 2013.

683 Trainer, M., Parrish, D. D., Buhr, M. P., Norton, R. B., Fehsenfeld, F. C., Anlauf, K. G., Bottenheim, J. W., Tang, Y. Z.,  
684 Wiebe, H. A., Roberts, J. M., Tanner, R. L., Newman, L., Bowersox, V. C., Meagher, J. F., Olszyna, K. J., Rodgers, M.  
685 O., Wang, T., Berresheim, H., Demerjian, K. L., and Roychowdhury, U. K.: Correlation of O<sub>3</sub> with NO<sub>y</sub> in  
686 photochemically aged air, *J. Geophys. Res.*, 98, 2917-2925, 1993.

687 Wang, R., Tao, S., Ciais, P., Shen, H. Z., Huang, Y., Chen, H., Shen, G. F., Wang, B., Li, W., Zhang, Y. Y., Lu, Y., Zhu, D.,  
688 Chen, Y. C., Liu, X. P., Wang, W. T., Wang, X. L., Liu, W. X., Li, B. G., and Piao, S. L.: High-resolution mapping of  
689 combustion processes and implications for CO<sub>2</sub> emissions, *Atmos. Chem. Phys.*, 13, 10, 5189-5203, 2013.

690 Wang, G., Huang, L., Gao, S., Gao, S., and Wang, L.: Characterization of water-soluble species of PM<sub>10</sub> and PM<sub>2.5</sub> aerosols  
691 in urban area in Nanjing, China, *Atmos. Environ.*, 36, 1299-1307, 2002.

692 Wang, G., Wang, H., Yu, Y., Gao, S., Feng, J., Gao, S., and Wang, L.: Chemical characterization of water-soluble  
693 components of PM<sub>10</sub> and PM<sub>2.5</sub> atmospheric aerosols in five locations of Nanjing, China, *Atmos. Environ.*, 37, 2893-  
694 2902, 2003.

695 Wang, T., Cheung, V. T. F., Anson, M., and Li, Y. S.: Ozone and related gaseous pollutants in the boundary layer of eastern  
696 China: overview of the recent measurements at a rural site, *Geophys. Res. Lett.*, 28, 2373-2376, 2001.

697 Wang, T., Wong, C. H., Cheung, T. F., Blake, D. R., Arimoto, R., Baumann, K., Tang, J., Ding, G. A., Yu, X. M., Li, Y. S.,  
698 Streets, D. G., and Simpson, I. J.: Relationships of trace gases and aerosols and the emission characteristics at Lin'an, a  
699 rural site in eastern China, during spring 2001, *J. Geophys. Res.*, 109, 19, 2004.

700 Wang, Y., Ying, Q., Hu, J., and Zhang, H.: Spatial and temporal variations of six criteria air pollutants in 31 provincial  
701 capital cities in China during 2013-2014, *Environ. Int.*, 73, 413-422, 2014.

702 Wang, Y. Q., Zhang, X. Y., Arimoto, R., Cao, J. J., and Shen, Z. X.: The transport pathways and sources of PM<sub>10</sub> pollution  
703 in Beijing during spring 2001, 2002 and 2003, *Geophys. Res. Lett.*, 31, L14110, 2004.

704 Wu, J., Xu, C., Wang, Q., and Cheng, W.: Potential sources and formations of the PM<sub>2.5</sub> pollution in urban Hangzhou,  
705 *Atmosphere*, 7, 100, 2016a.

706 Wu, Y., Hu, M., Zeng, L., Dong, H., Li, X., Lu, K., Lu, S., Yang, Y., and Zhang, Y.: Seasonal variation of trace gas  
707 compounds and PM<sub>2.5</sub> observed at an urban supersite in Beijing, EGU General Assembly Conference Abstracts, 12409,  
708 2016b.

709 Xue, L. K., Wang, T., Gao, J., Ding, A. J., Zhou, X. H., Blake, D. R., Wang, X. F., Saunders, S. M., Fan, S. J., Zuo, H. C.,  
710 Zhang, Q. Z., and Wang, W. X.: Ground-level ozone in four Chinese cities: precursors, regional transport and  
711 heterogeneous processes, *Atmos. Chem. Phys.*, 14, 13175-13188, 2014.

712 Xue, L. K., Wang, T., Louie, P. K. K., Luk, C.W. Y., Blake, D. R., Xu, Z.: Increasing external effects negate local efforts to  
713 control ozone air pollution: a case study of Hong Kong and implications for other Chinese cities, *Environ. Sci. Tech.*,  
714 48(18), 10769-10775, 2014.

715 Yang, L. X., Cheng, S. H., Wang, X. F., Nie, W., Xu, P. J., Gao, X. M., Yuan, C., and Wang, W. X.: Source identification  
716 and health impact of PM<sub>2.5</sub> in a heavily polluted urban atmosphere in China, *Atmos. Environ.*, 75, 265-269, 2013.

717 Yu, S. C., Zhang, Q. Y., Yan, R. C., Wang, S., Li, P. F., Chen, B. X., Liu, W. P., and Zhang, X. Y.: Origin of air pollution  
718 during a weekly heavy haze episode in Hangzhou, China, *Environ. Chem. Lett.*, 12, 543-550, 2014.

719 Zhang, H. L., Li, J. Y., Ying, Q., Yu, J. Z., Wu, D., Cheng, Y., He, K. B., and Jiang, J. K.: Source apportionment of PM<sub>2.5</sub>  
720 nitrate and sulfate in China using a source-oriented chemical transport model, *Atmos. Environ.*, 62, 228-242, 2012.

721 Zhang, L. M., Gong, S. L., Padro, J., and Barrie, L.: A size segregated particulate dry deposition scheme for an atmospheric  
722 aerosol module, *Atmos. Environ.*, 35, 549-560, 2001.

723 Zhang, R, Jing, J., Tao, J., Hsu, S. C., Wang, G., Cao, J., Lee, C. S. L., Zhu, L., Chen, Z., Zhao, Y., and Shen, Z.: Chemical  
724 characterization and source apportionment of PM<sub>2.5</sub> in Beijing: seasonal perspective, *Atmos. Chem. Phys.*, 13, 7053-  
725 7074, 2013.

726 Zhang, R. Y., Suh, I., Zhao, J., Zhang, D., Fortner, E. C., Tie, X. X., Molina, L. T., and Molina, M. T.: Atmospheric new  
727 particulate formation enhanced by organic acids, *Science*, 304, 5676, 1487-1490, 2004.

728 Zhang, Q., Yuan, B., Shao, M., Wang, X., Lu, S., Lu, K., Wang, M., Chen, L., Chang, C.-C., and Liu, S. C.: Variations of  
729 ground-level O<sub>3</sub> and its precursors in Beijing in summertime between 2005 and 2011, *Atmos. Chem. Phys.*, 14, 6089-  
730 6101, 2014.

731 Zhang, Q., Streets, D. G., Carmichael, G. R., He, K. B., Huo, H., Kannari, A., Klimont, Z., Park, I. S., Reddy, S., Fu, J. S.,  
732 Chen, D., Duan, L., Lei, Y., Wang, L. T., and Yao, Z. L.: Asian emissions in 2006 for the NASA INTEX-B mission,  
733 *Atmos. Chem. Phys.*, 9, 5131-5153, 2009.

734 Zhong, Q. R., Huang, Y., Shen, H. Z., Chen, Y. L., Chen, H., Huang, T. B., Zeng, E. Y., and Tao, S.: Global estimates of  
735 carbon monoxide emissions from 1960 to 2013, *Environ. Sci. Pollut. Res.*, 24, 864-873, 2014.

736

737 Table 1 Statistics of general meteorological parameters at NRCS for the period during January- December 2013\*.

Month	Temperature (°C)	RH (%)	Wind Speed (m s <sup>-1</sup> )	Rainfall (mm)	Pressure (Pa)	Visibility (m)
Jan.	4.5 ± 3.4	76 ± 9	1.9	24.9	10221.6	2566.0
Feb.	7.0 ± 4.3	81 ± 6	2.3	66.8	10197.2	3511.8
Mar.	12.3 ± 4.2	67 ± 15	2.7	115.9	10140.5	5459.1
Apr.	16.9 ± 3.9	56 ± 17	2.6	98.1	10095.3	7587.8
May	23.0 ± 3.0	69 ± 13	2.1	121.3	10045.8	6118.9
Jun.	24.7 ± 3.1	78 ± 7	2.0	346	10013.0	5693.5
Jul.	32.3 ± 1.6	51 ± 7	2.8	9.3	9997.8	17011.0
Aug.	31.3 ± 2.7	58 ± 14	2.6	212.1	10001.7	13958.3
Sep.	25.0 ± 2.7	73 ± 11	2.3	49.4	10015.2	9584.7
Oct.	19.3 ± 2.8	73 ± 11	2.5	331	10146.1	7551.8
Nov.	13.5 ± 3.9	68 ± 16	1.9	32.6	10178.8	5759.2
Dec.	6.3 ± 3.6	64 ± 15	2.0	82.7	10208.6	3941.2

738 \*Note: average values for air temperature (T), relative humidity (RH), wind speed (WS), pressure, and visibility and  
739 accumulated monthly value for rainfall, respectively.

740



741 Table 2 Mean species levels for different seasons and different time of day and comparisons with other previous data  
 742 reported in typical regions in China.

Species	Areas	Location	Period	The whole day			Day time (08:00-17:00)			Night time (18:00-07:00)		
				Mean	SD	Max	Mean	SD	Max	Mean	SD	Max
PM <sub>2.5</sub> (ug m <sup>-3</sup> )	This study	YRD	DJF	74.2	49.3	406.4	75.1	50.5	406.4	73.6	48.4	325.5
			MAM	47.1	26.2	201.1	47.7	26.6	201.1	46.7	25.9	154.0
			JJA	34.6	22.5	181	35.1	25.7	181.0	34.3	20.0	139.6
			SON	52.5	34.4	272.4	51.7	33.3	238.1	53.1	35.1	272.4
				<sup>a</sup> Xiacheng District, Hangzhou (Sep.-Nov. 2013) monthly mean: 69 µg m <sup>-3</sup>								
				<sup>b</sup> NRCS, Hangzhou (2012) annual mean: 50.0 µg m <sup>-3</sup>								
				<sup>c</sup> Hangzhou (Sep. 2010-Nov. 2011 during non-raining days) annual average: 106-131 µg m <sup>-3</sup>								
				<sup>d</sup> Nine sites in Nanjing (2013) AM: 55-60 µg m <sup>-3</sup> , JJA: 30-60 µg m <sup>-3</sup> , SON: 55-85 µg m <sup>-3</sup>								
				<sup>e</sup> Nanjing (Mar. 2013-Feb. 2014) annual mean: 75±50 µg m <sup>-3</sup>								
				<sup>e</sup> Shanghai (Mar. 2013-Feb. 2014) annual mean: 56 ± 41 µg m <sup>-3</sup>								
	BTH		<sup>e</sup> Beijing (Mar. 2013-Feb. 2014) annual mean: 87±67 µg m <sup>-3</sup>									
	PRD		<sup>e</sup> Guangzhou (Mar. 2013-Feb. 2014) annual mean: 52±28 µg m <sup>-3</sup>									
PM <sub>10</sub> (ug m <sup>-3</sup> )	This study	YRD	DJF	113.1	71.7	589.6	115.3	73.6	589.6	111.5	70.4	481.6
			MAM	77.1	42.3	484.1	79.3	41.0	249.1	75.6	43.2	484.1
			JJA	54.9	31.6	231.4	55.7	34.8	231.4	54.4	29.2	183.8
			SON	85.6	51.2	344.2	84.8	48.6	341.3	86.1	53.0	344.2
				<sup>e</sup> Hangzhou (Mar. 2013-Feb. 2014) annual mean: 98 ± 59 µg m <sup>-3</sup>								
				<sup>c</sup> Hangzhou (Sep. 2010-Nov. 2011 during non-raining days) annual average: 127-158 µg m <sup>-3</sup>								
				<sup>f</sup> Hangzhou (Sep. 2001-Aug. 2002) annual mean: 119.2 µg m <sup>-3</sup>								
				<sup>e</sup> Nanjing (Mar. 2013-Feb. 2014) annual mean: 134 ± 73 µg m <sup>-3</sup>								
				<sup>e</sup> Shanghai (Mar. 2013-Feb. 2014) annual mean: 80 ± 47 µg m <sup>-3</sup>								
		BTH		<sup>e</sup> Beijing (Mar. 2013-Feb. 2014) annual mean: 109±62 µg m <sup>-3</sup>								
	PRD		<sup>e</sup> Guangzhou (Mar. 2013-Feb. 2014) annual mean: 72±35 µg m <sup>-3</sup>									
O <sub>3</sub> (ppbv)	This study	YRD	DJF	13.8	13.1	70.9	17.7	14.1	70.9	10.2	10.9	58.5
			MAM	29.8	24.0	141.2	42.4	27.3	141.2	20.0	15.1	105.9
			JJA	31.3	26.0	145.4	48.8	26.6	145.4	18.2	15.8	118.7
			SON	25.9	22.5	100.1	37.0	25.1	100.1	16.3	14.3	99.5
				<sup>e</sup> Hangzhou (Mar. 2013-Feb. 2014) annual mean: 44 ± 21 ppbv (8 h O <sub>3</sub> )								
				<sup>e</sup> Nanjing (Mar. 2013-Feb. 2014) annual mean: 42 ± 20 ppbv (8 h O <sub>3</sub> )								
				<sup>e</sup> Shanghai (Mar. 2013-Feb. 2014) annual mean: 48 ± 21 ppbv (8 h O <sub>3</sub> )								
		BTH		<sup>e</sup> Beijing (Mar. 2013-Feb. 2014) annual mean: 45 ± 27 ppbv (8 h O <sub>3</sub> )								
		PRD		<sup>e</sup> Guangzhou (Mar. 2013-Feb. 2014) annual mean: 45 ± 24 ppbv (8 h O <sub>3</sub> )								
	SO <sub>2</sub> (ppbv)	YRD	This study	DJF	14.5	10.2	71.2	16.2	10.2	71.2	13.3	10.2

		MAM	11.3	9.1	75.1	11.7	9.6	75.1	11.0	8.7	59.3	
		JJA	8.6	6.5	51.0	8.0	6.3	51.0	9.0	6.6	46.7	
		SON	9.6	7.2	63.8	10.3	7.1	58.3	9.0	7.3	63.8	
		<sup>a</sup> Hangzhou Xiacheng District (12-19 Oct., 2013) daily mean: 5.7-9.7 ppbv										
		<sup>e</sup> Hangzhou (Mar. 2013-Feb. 2014) annual mean: 9 ± 4 ppbv										
		<sup>e</sup> Nanjing (Mar. 2013-Feb. 2014) annual mean: 12 ± 6 ppbv										
		<sup>e</sup> Shanghai (Mar. 2013-Feb. 2014) annual mean: 7 ± 5 ppbv										
	BTH	<sup>e</sup> Beijing (Mar. 2013-Feb. 2014) annual mean: 9 ± 8 ppbv										
	PRD	<sup>e</sup> Guangzhou (Mar. 2013-Feb. 2014) annual mean: 7 ± 3 ppbv										
CO (ppmv)	YRD		DJF	1.4	0.7	3.8	1.4	0.7	3.3	1.4	0.7	3.8
		This study	MAM	0.7	0.2	2.2	0.7	0.3	2.2	0.7	0.2	1.7
			JJA	0.5	0.2	2.0	0.5	0.2	1.9	0.5	0.2	2.0
			SON	0.8	0.3	3.4	0.7	0.3	1.9	0.8	0.3	3.4
		<sup>e</sup> Hangzhou (Mar. 2013-Feb. 2014) annual mean: 0.7 ± 0.3 ppmv										
		<sup>e</sup> Nanjing (Mar. 2013-Feb. 2014) annual mean: 0.8 ± 0.4 ppmv										
		<sup>e</sup> Shanghai (Mar. 2013-Feb. 2014) annual mean: 0.7 ± 0.3 ppmv										
	BTH	<sup>e</sup> Beijing (Mar. 2013-Feb. 2014) annual mean: 1.1 ± 0.7 ppmv										
	PRD	<sup>e</sup> Guangzhou (Mar. 2013-Feb. 2014) annual mean: 0.8 ± 0.2 ppmv										
	NO <sub>2</sub> (ppbv)	YRD		DJF	37.4	20.1	146.9	35.7	19.5	126.3	38.5	20.5
This study			MAM	28.7	12.9	94.8	25.3	12.1	94.8	31.0	12.9	87.4
			JJA	17.3	10.2	61.4	13.0	9.2	46.1	20.3	9.7	61.4
			SON	28.4	15.2	94.1	25.1	13.3	86.2	30.7	16.0	94.1
		<sup>e</sup> Hangzhou (Mar. 2013-Feb. 2014) annual mean: 13 ± 9 ppbv										
		<sup>e</sup> Nanjing (Mar. 2013-Feb. 2014) annual mean: 26 ± 11 ppbv										
		<sup>e</sup> Shanghai (Mar. 2013-Feb. 2014) annual mean: 20 ± 9 ppbv										
BTH		<sup>e</sup> Beijing (Mar. 2013-Feb. 2014) annual mean: 25 ± 11 ppbv										
PRD		<sup>e</sup> Guangzhou (Mar. 2013-Feb. 2014) annual mean: 24 ± 10 ppbv										
NO <sub>x</sub> (ppbv)		YRD		DJF	60.5	34.7	199.8	58.0	32.1	168.9	62.3	36.3
	This study		MAM	40.0	19.8	131.4	36.5	19.2	129.2	42.5	19.8	131.4
			JJA	24.3	14.8	99.6	18.6	14.1	99.6	28.2	14.0	83.1
			SON	41.0	24.3	153.4	36.6	21.1	123.7	44.2	25.8	153.4
NO <sub>y</sub> (ppbv)	YRD		DJF	84.7	48.4	295.2	82.4	44.6	263.7	86.4	51.1	295.2
		This study	MAM	66.0	33.6	248.8	62.9	34.6	248.8	68.2	32.8	204.1
			JJA	43.6	27.6	259.5	36.8	29.3	259.5	48.5	25.2	167.7
			SON	70.2	37.9	319.3	65.5	35.6	319.3	73.6	39.1	251.8
	<sup>g</sup> Nanjing SORPES 2013 monthly mean: 30-70 ppbv											
	<sup>h</sup> Shanghai May-June 2005 daily mean: 24-39 ppbv											

---

BTH <sup>a</sup>Beijing 2011-2015 annual mean: 54.6 ± 4.7 ppbv

YRD <sup>h</sup>Guangzhou Apr.-May 2004: 24-52 ppbv

---

743 <sup>a</sup> Wu et al. (2016a); <sup>b</sup> Qi et al. (2015); <sup>c</sup> Sun et al. (2013); <sup>d</sup> Chen et al. (2016); <sup>e</sup> Wang et al. (2014); <sup>f</sup> Cao et al. (2009); <sup>g</sup> Ding  
744 et al. (2013); <sup>h</sup> Xue et al. (2014)

745 Table 3 Mean concentrations of PM<sub>2.5</sub> (µg m<sup>-3</sup>) and other trace gases (ppmv unit for CO but ppbv for other gases) in the  
 746 identified trajectory clusters within four season period, together with the percentages of each trajectory cluster.

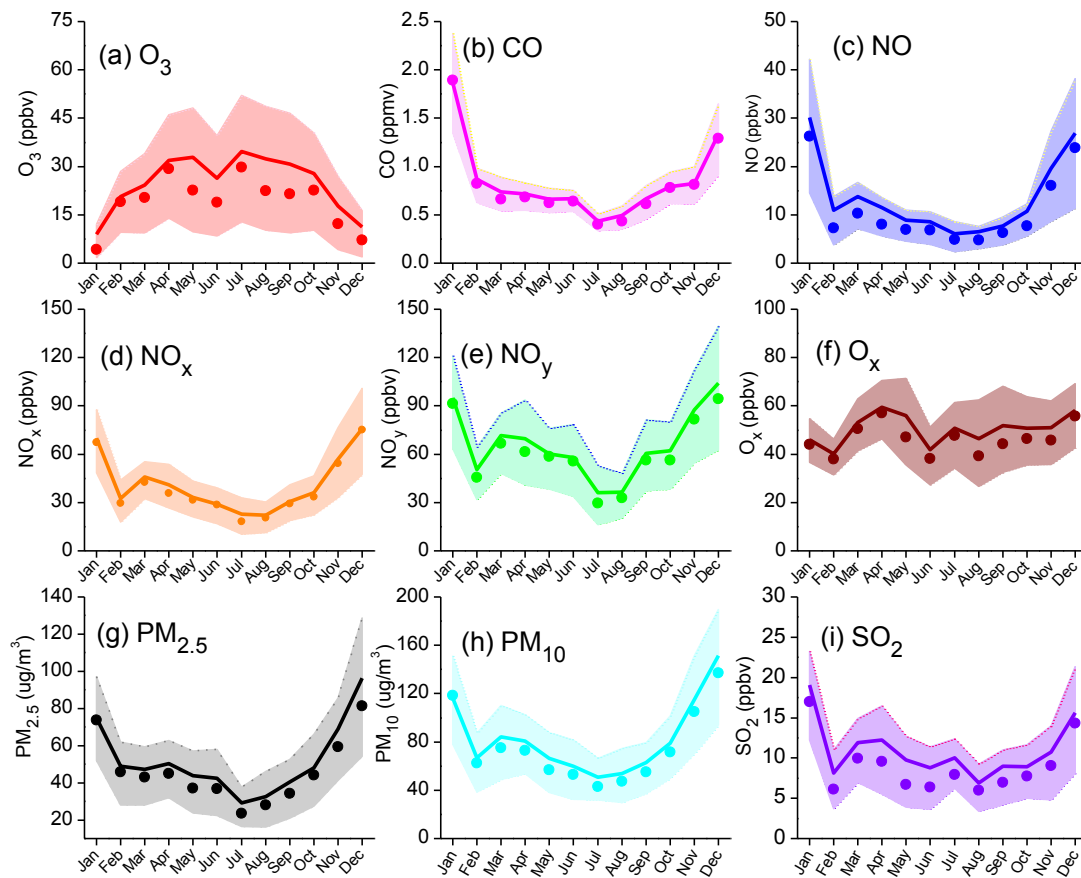
Season	Cluster	Percent (%)	PM <sub>2.5</sub>	O <sub>3</sub>	SO <sub>2</sub>	CO	NO <sub>x</sub>
Spring	1	12.05	45.0	28.3	10.7	0.7	38.3
	2	16.58	44.3	31.6	13.2	0.7	39.1
	3	16.03	35.3	30.5	9.7	0.6	34.5
	4	42.66	52.4	23.2	11.4	0.8	42.5
	5	5.53	38.2	34.2	11.2	0.7	37.9
	6	7.16	58.1	34.2	11.9	0.8	43.8
Summer	1	8.42	51.5	24.6	7.9	0.8	29.2
	2	8.61	34.2	35.2	9.2	0.5	22.8
	3	22.55	24.0	28.7	7.9	0.4	21.7
	4	31.34	38.2	36.8	9.1	0.5	24.4
	5	19.38	38.7	27.2	8.9	0.6	28.7
	6	9.69	22.4	26.7	7.5	0.4	17.6
Autumn	1	23.63	42.1	27.4	9.9	0.7	36.9
	2	32.51	50.7	24.6	8.2	0.8	39.4
	3	8.33	21.7	19.8	8.0	0.5	22.0
	4	7.78	68.6	34.8	8.4	0.8	38.8
	5	11.90	49.9	22.6	10.1	0.7	40.8
	6	15.84	79.6	21.6	12.9	0.9	62.0
Winter	1	7.13	60.9	16.6	15.4	1.3	53.7
	2	24.26	83.3	14.4	15.9	1.4	65.4
	3	16.39	47.3	14.0	11.9	1.1	42.7
	4	21.76	75.9	11.9	13.5	1.5	63.1
	5	16.76	67.0	11.7	13.1	1.5	53.7
	6	13.70	102.1	14.4	16.9	1.4	81.0



747

748

Fig. 1. Location of NRCS station in YRD region (left) and in the city of Hangzhou (right top).



749

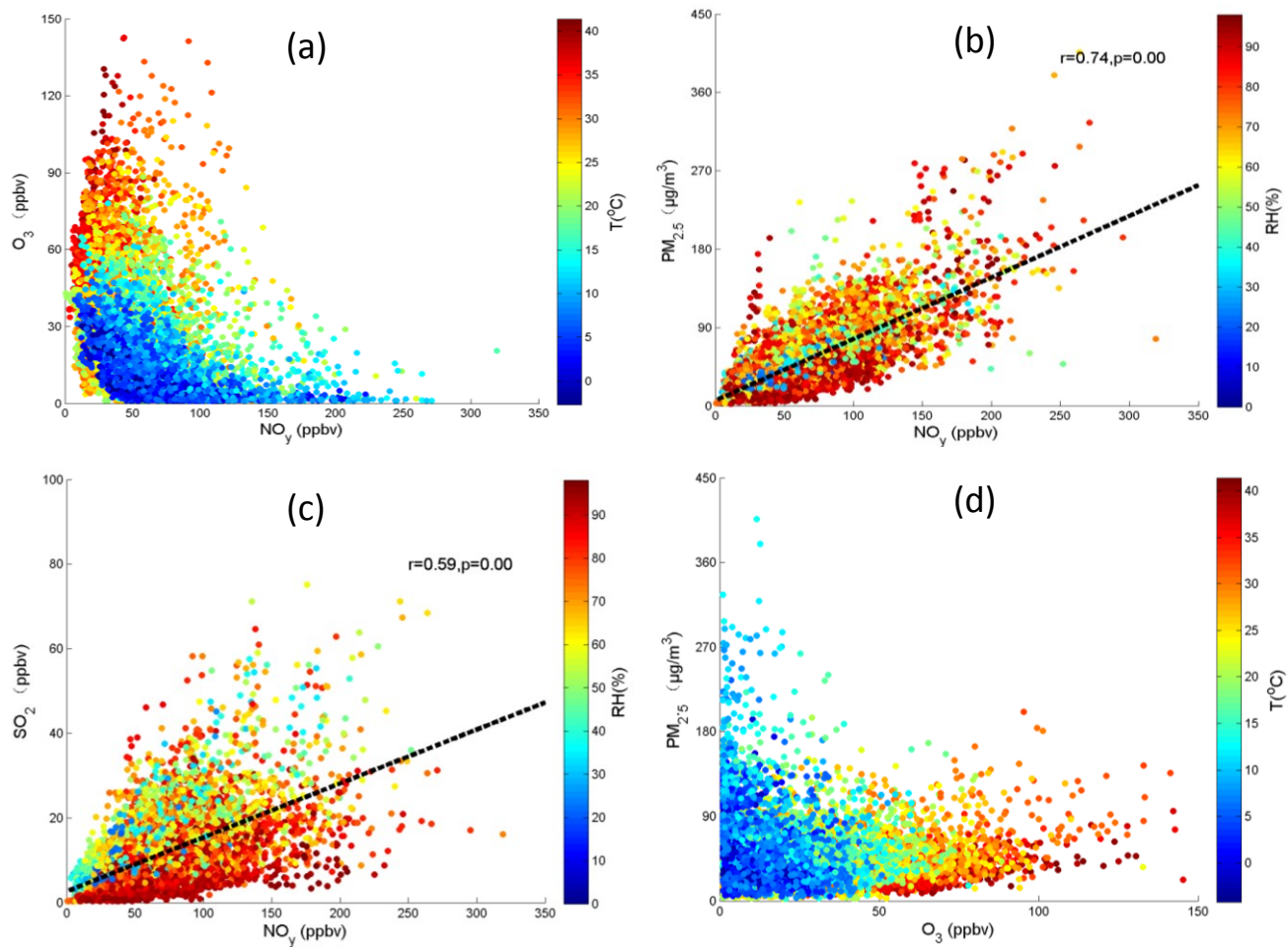
750 Fig. 2. Seasonal variations of atmospheric O<sub>3</sub> (a), CO (b), NO (c), NO<sub>x</sub> (d), NO<sub>y</sub> (e), O<sub>x</sub> (f), PM<sub>2.5</sub> (g), PM<sub>10</sub> (h), and SO<sub>2</sub> (i).

751 Bold solid lines are the monthly averages, solid circles are the median values, and thin lines represent percentiles of 75% and

752

25%.

753



754

755 Fig. 3. Scatter plots of  $NO_y$  with  $O_3$  ( $NO_y$ - $O_3$ ) coded with air temperature (a),  $NO_y$ - $PM_{2.5}$  coded with relative humidity (b),  
 756  $NO_y$ - $SO_2$  coded with relative humidity (c), and  $O_3$ - $PM_{2.5}$  coded with air temperature (d).

757

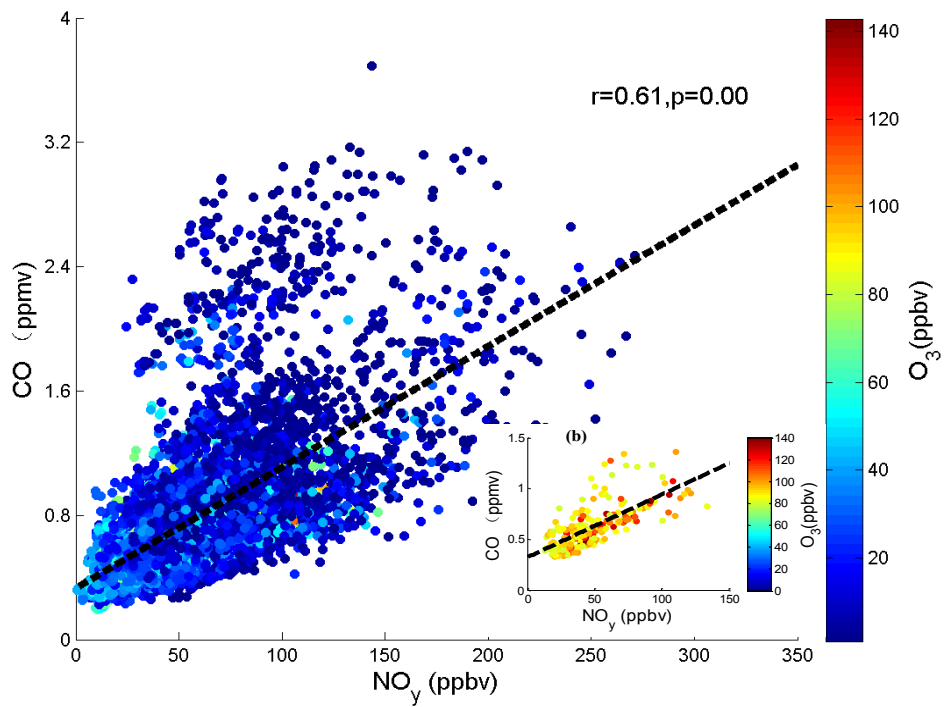
758

759

760

761

762



763

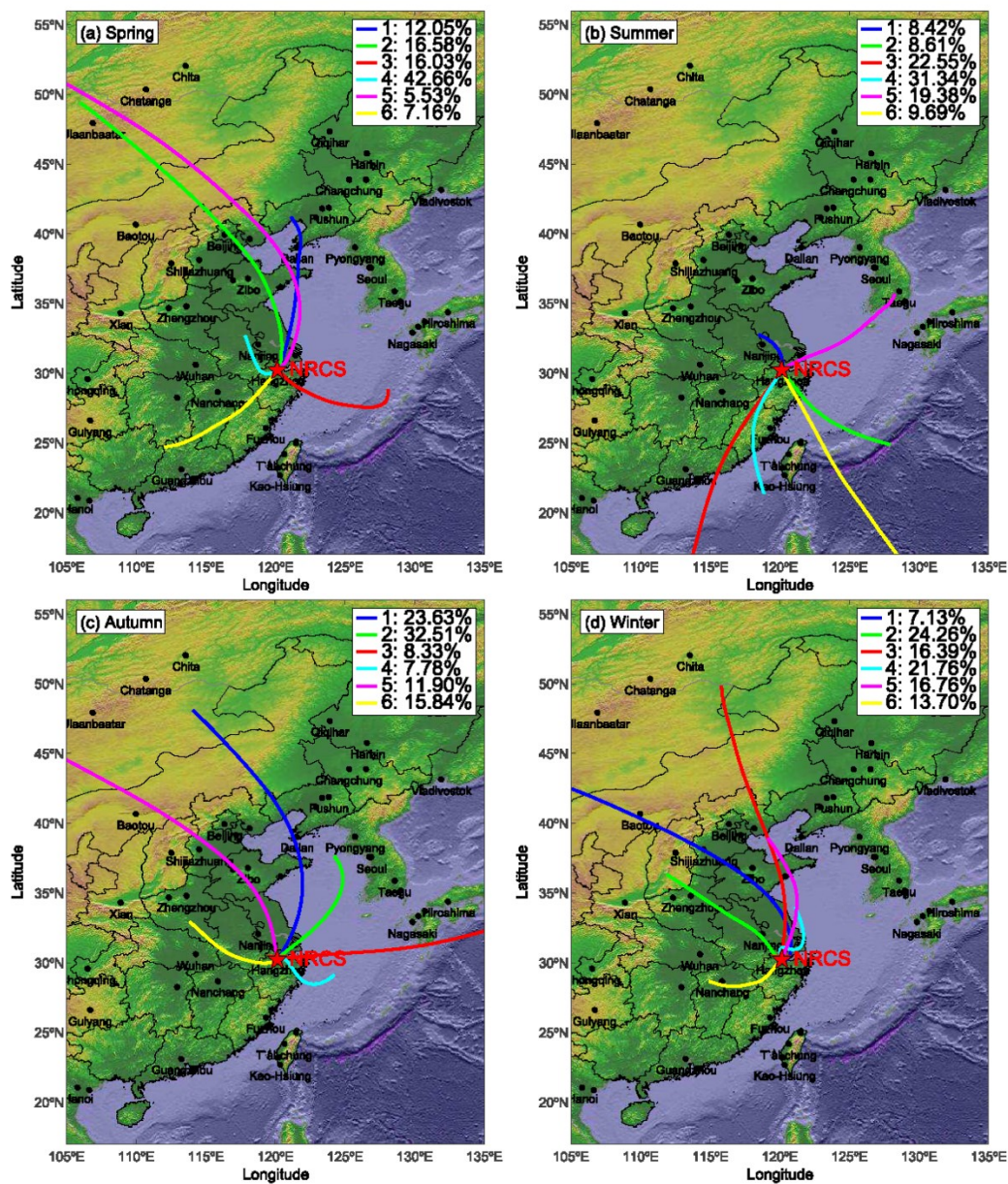
764

Fig. 4. Scatter plots of NO<sub>y</sub> with CO coded with O<sub>3</sub> mixing ratios, along the subpicture (b) showing the scatter with O<sub>3</sub> mixing ratios above 80 ppbv.

765

766

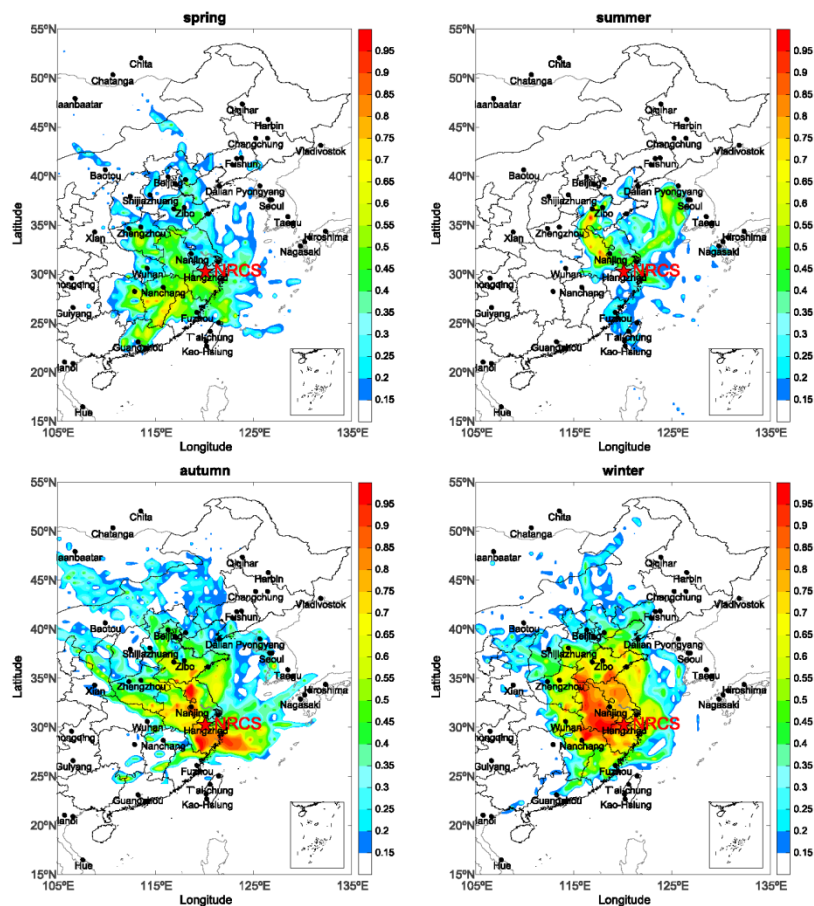




767

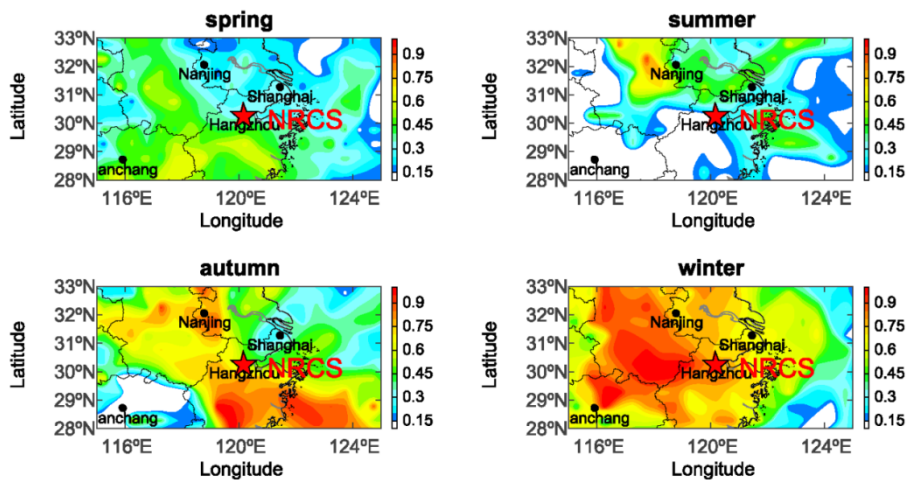
768

Fig. 5. Seasonal cluster analysis of the 72-h air mass back trajectories starting at 100 m from NRCS site in Hangzhou.



769

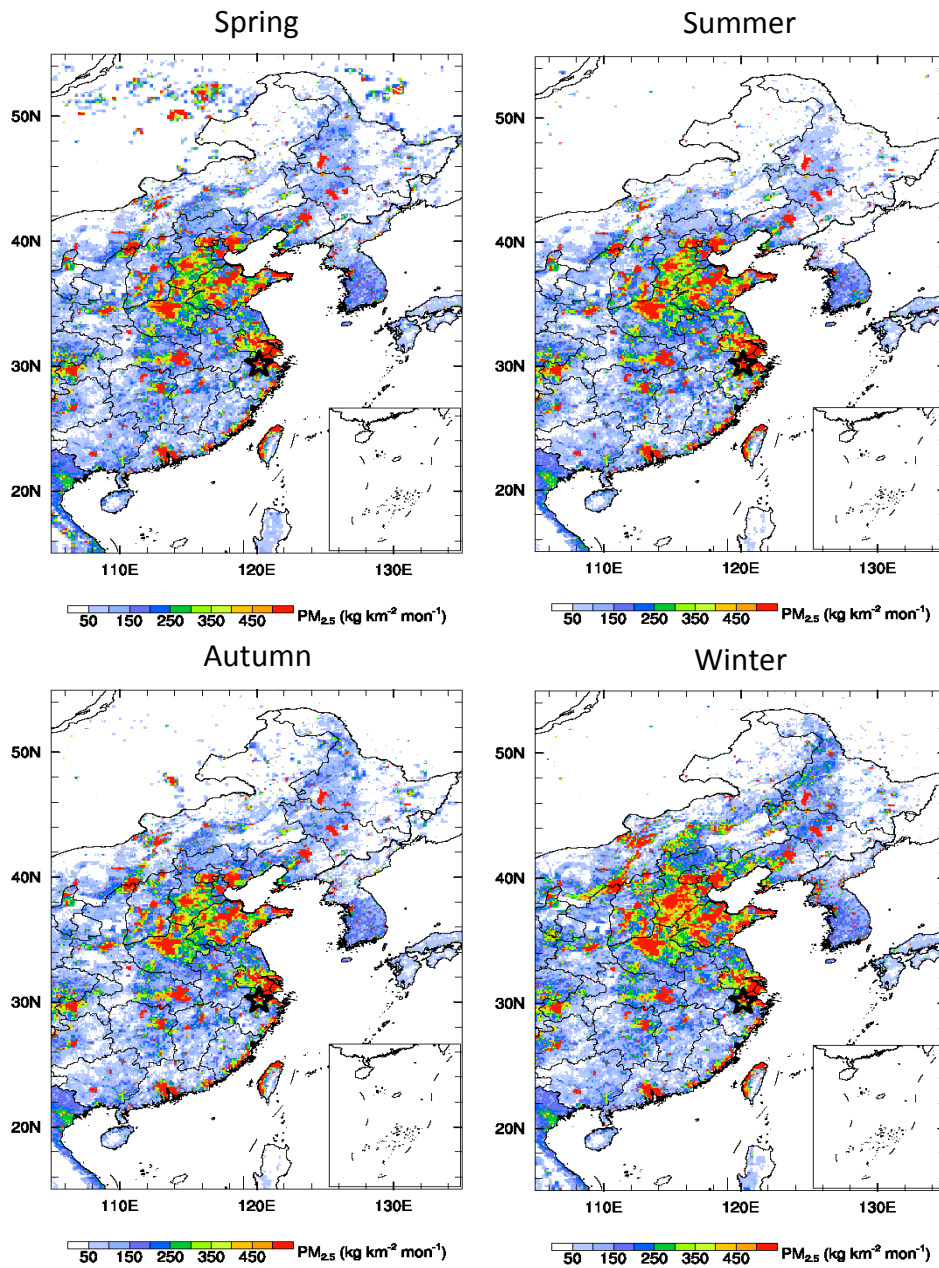
770 Fig. 6a. Seasonal weighted potential source contribution function (WPSCF) maps of  $PM_{2.5}$  in Hangzhou. The sampling site is  
 771 marked in pentacle and the WPSCF values are displayed in color.



772

773

Fig. 6b. The zoomed view of Fig. 6a.



774

775 Fig. 6c. Seasonal and spatial distributions of PM<sub>2.5</sub> emissions (kg km<sup>2</sup> mon<sup>-1</sup>) at the surface layer in China. The sampling site

776

is marked in pentacle.

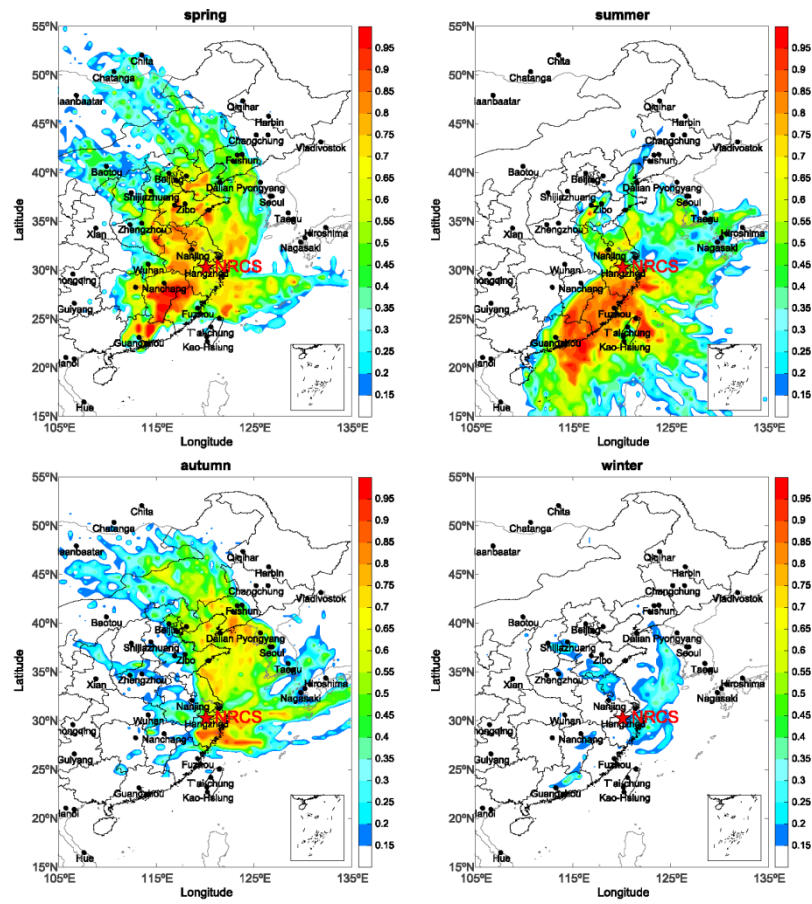


Fig. 7a. Same as Fig. 6a but for O<sub>3</sub>

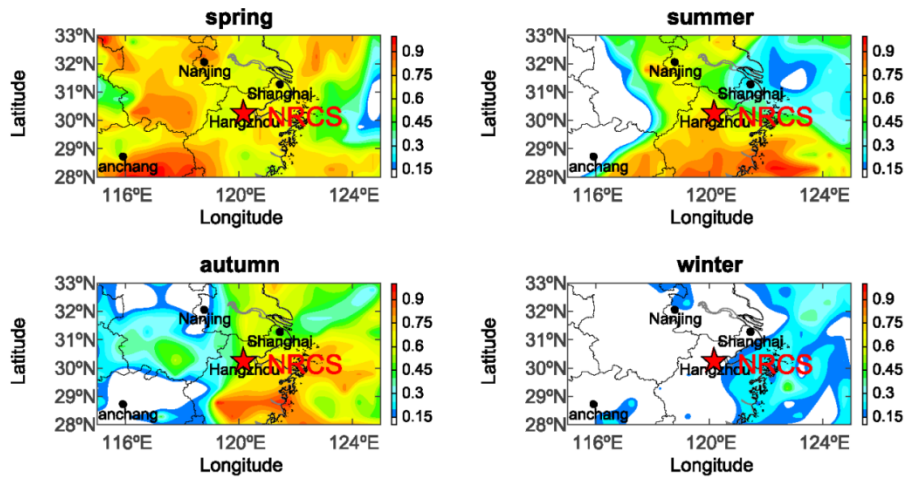


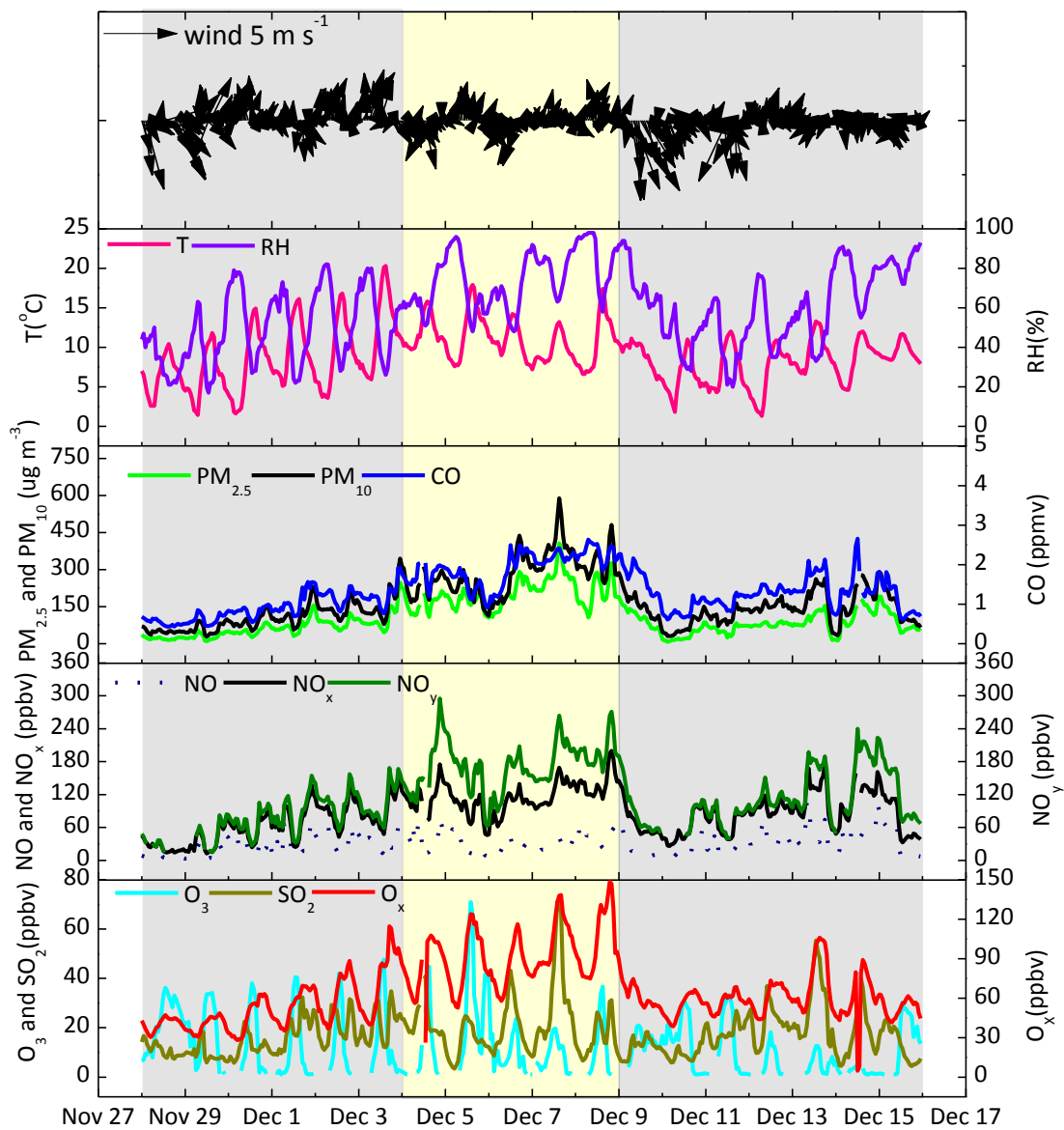
Fig. 7b The zoomed view of Fig. 7a

777

778

779

780

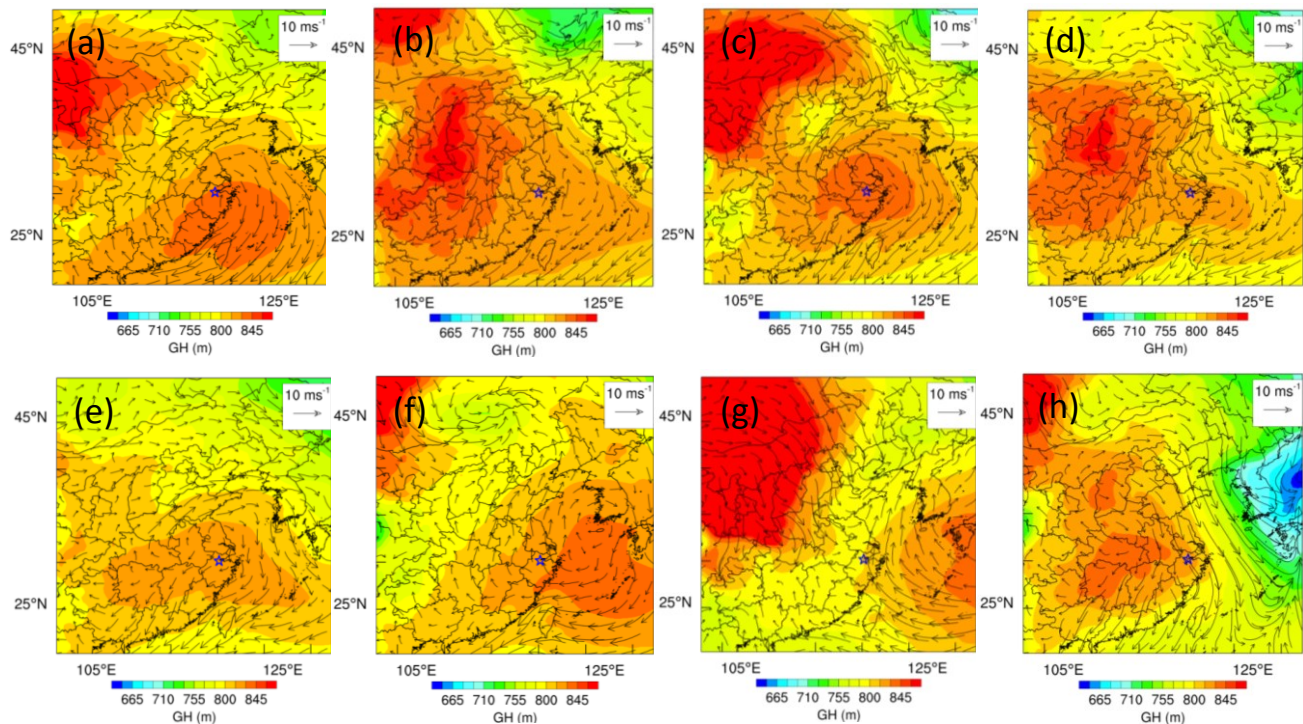


781

782 Fig. 8. Time series of meteorological parameters and chemical species before, during, and after haze period. The gray shaded

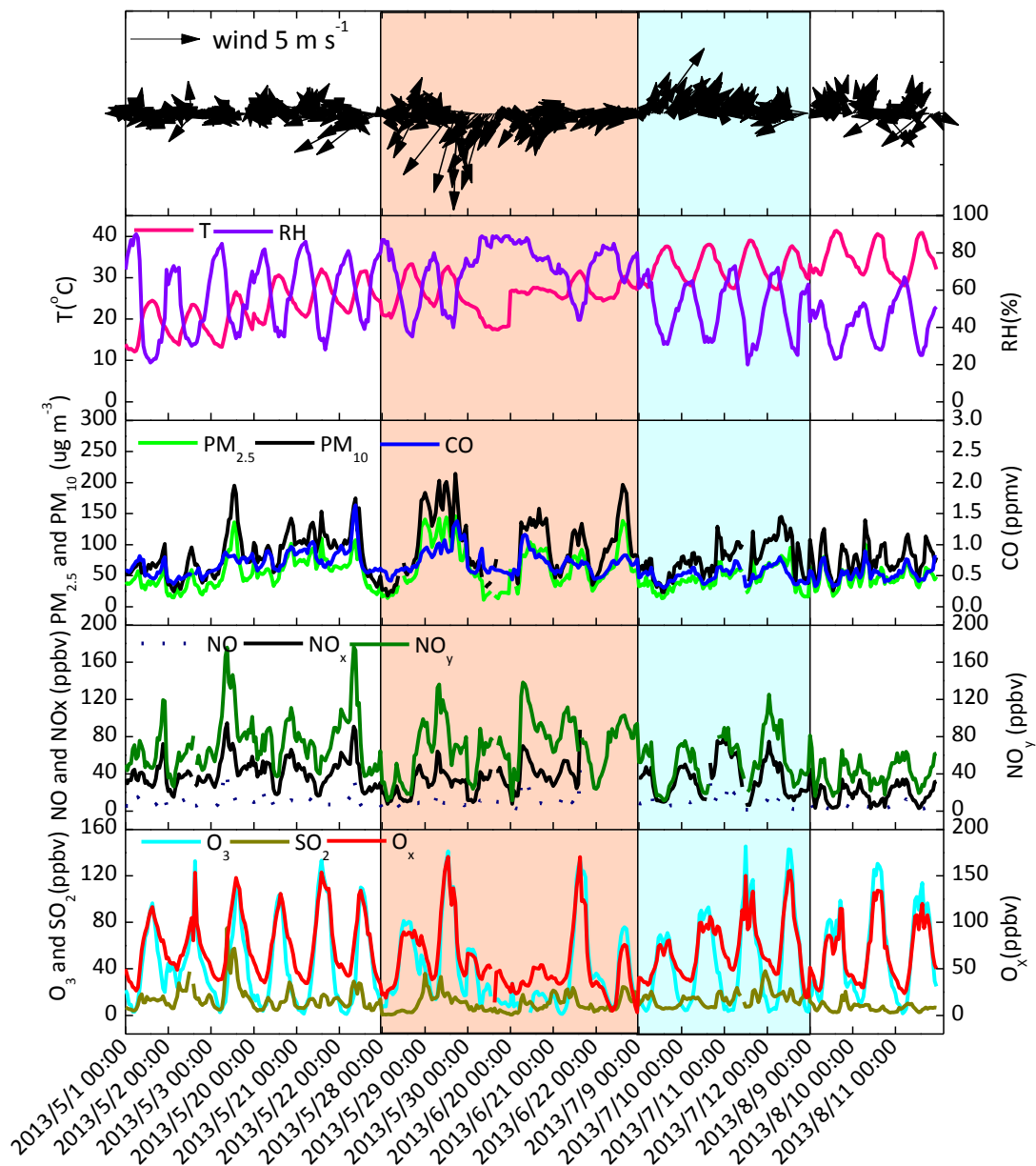
783 area indicates the Phase I (28 Nov.-3 Dec.) and II (10-12 Dec.) and the orange shaded area represents haze events Phase III

784 (2-9 Dec.) and IV (13-15 Dec.).



785

786 Fig. 9. The Geopotential Height Field (GH) (indicated by color bars) and Wind Field (WF) (black vectors) for 925 hPa at  
 787 20:00 LT during 2-9 December, 2013. Fig. 12a-d and Fig. 12e-h represent for 2-5 December and 6-9 December from left to  
 788 right on the top and bottom, respectively. The NRCS station was marked by pentagram.



789

790 Fig. 10. Same as Fig. 8 but during photochemical pollution period. The orange shaded area represents the Phase I (28-30  
 791 May and 20-22 June), the cyan shaded area indicates the Phase II (9-12 July), and the other area represents the Phase III (1-3  
 792 May, 20-22 May, and 9-11 August)